AD-A165 203 THE DELAYED FRACTURE OF ALUMINUM ALLOYS(U) MARTIN MARIETTA LABS BALTIMORE MD J R PICKENS ET AL. OCT 85 MML-TR-85-64C N00014-83-C-0380 1/1

UNCLASSIFIED F/G 11/6 NL

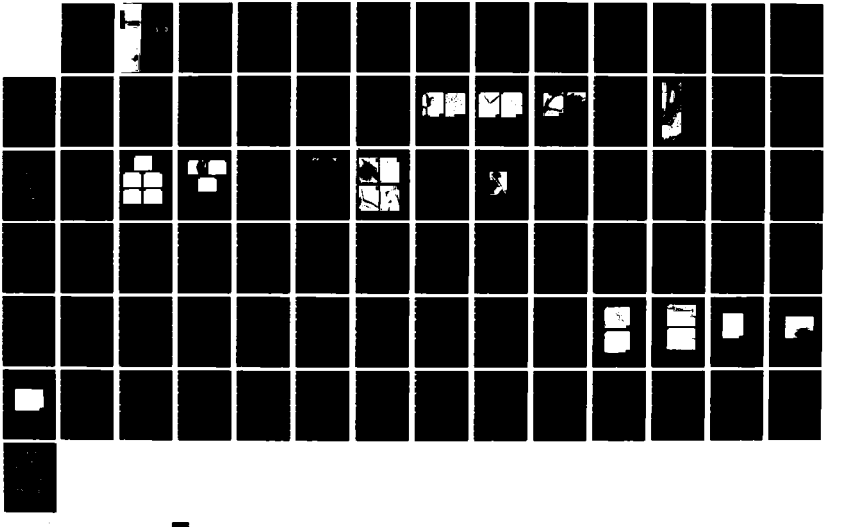

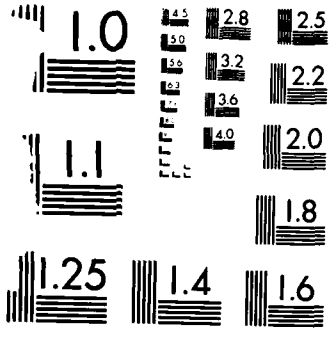

MICROCOPY RESOLUTION TEST CHART
NATIONAL BUREAU OF STANDARDS-1963-A

(12)

RTIN MARIETTA

rtin Marietta
Laboratories

MMLTR85-64c

THE DELAYED FRACTURE OF ALUMINUM ALLOYS

Final Report

October 1985

Prepared for Contract
N00014-83-C-0380
Office of Naval Research
Department of the Navy
800 North Quincy Street
Arlington, Virginia 22217

Prepared by:

J.R. Pickens and T.J. Langan
MARTIN MARIETTA CORPORATION
Martin Marietta Laboratories
1450 South Rolling Road
Baltimore, Maryland 21227

SUMMARY

The role of grain boundary (GB) segregation in the mechanism of stress-corrosion cracking (SCC) of Al-Zn-Mg alloys was studied using Auger electron spectroscopy and bolt-loaded double-cantilever beam specimens in a saline solution. Several environments were investigated for inducing intergranular fracture and thus exposing the GB surface for examination. The following technique was developed to induce fracture on the actual GB surface: specimens are pre-exposed to water vapor-saturated air at 1 atmosphere (gauge), which charges hydrogen into the material, causing intergranular hydrogen embrittlement. Specimens are then fractured under ultra-high vacuum, and the surface compositions of the resulting fracture surfaces are analyzed using a scanning Auger microprobe (SAM).

We endeavored to vary GB segregation, and possibly SCC susceptibility, by varying the solution heat-treatment temperature (SHT) of an extremely susceptible Al-6.9Zn-3.0Mg-0.1Zr (wt%) high-purity alloy. The thermo-mechanical history of the alloy was carefully controlled to isolate SHT and its effect on GB segregation as a test variable. SCC susceptibility, as measured by plateau crack velocity (v_p), decreased with increasing SHT. This finding helps to resolve the existing controversy in the literature on the effect of SHT on SCC susceptibility.

Both Mg and Zn GB segregation were detected using the SAM. Moreover, free Mg -- i.e., not bound in the $MgZn_2$ GB precipitates -- was unequivocally shown to exist on the boundaries of this alloy in the highly susceptible peak-aged temper. However, no correlation between SCC susceptibility and GB segregation of free Mg was observed. Thus, the Mg-H interaction mechanism of SCC remains unproven.

The following two papers detail the aforementioned studies and constitute our end-of-contract report.

TABLE OF CONTENTS

Unclassified

SECURITY CLASSIFICATION OF THIS PAGE (When Data Entered)

REPORT DOCUMENTATION PAGE	READ INSTRUCTIONS BEFORE COMPLETING FORM
1. REPORT NUMBER MMLTR85-64(c)	2. GOVT ACCESSION NO. AD-A165203	3. RECIPIENT'S CATALOG NUMBER
4. TITLE (and Subtitle) The Delayed Fracture of Aluminum Alloys End-of-Contract Report	5. TYPE OF REPORT & PERIOD COVERED Final Report
	6. PERFORMING ORG. REPORT NUMBER MMLTR85-64(c)
7. AUTHOR(s) Joseph R. Pickens and Timothy J. Langan	8. CONTRACT OR GRANT NUMBER(s) N00014-83-C-0380
9. PERFORMING ORGANIZATION NAME AND ADDRESS Martin Marietta Corporation Martin Marietta Laboratories 1450 South Rolling Road, Baltimore, MD 21227	10. PROGRAM ELEMENT, PROJECT, TASK AREA & WORK UNIT NUMBERS
11. CONTROLLING OFFICE NAME AND ADDRESS	12. REPORT DATE October, 1985
	13. NUMBER OF PAGES
14. MONITORING AGENCY NAME & ADDRESS(if different from Controlling Office) Office of Naval Research Department of the Navy 800 North Quincy Street Arlington, Virginia 22217	15. SECURITY CLASS. (of this report) Unclassified
	15a. DECLASSIFICATION/DOWNGRADING SCHEDULE

16. DISTRIBUTION STATEMENT (of this Report)

Distribution of this document is unlimited.

17. DISTRIBUTION STATEMENT (of the abstract entered in Block 20, if different from Report)

18. SUPPLEMENTARY NOTES

19. KEY WORDS (Continue on reverse side if necessary and identify by block number)

Aluminum alloys, ~~7xxx~~ alloys, stress-corrosion cracking, intergranular fracture, grain boundary segregation, liquid metal embrittlement, hydrogen embrittlement, fracture at cryogenic temperatures, Auger electron spectroscopy, aging, solution heat treatment, insitu fracture.

20. ABSTRACT (Continue on reverse side if necessary and identify by block number)

The relationship between susceptibility to stress-corrosion cracking (SCC) and grain boundary (GB) chemistry was investigated in an attempt to elucidate the SCC mechanism in ~~Al-Zn-Mg~~ alloys. Research was performed in two phases: (1) develop a method for inducing intergranular fracture on the actual grain boundary to enable measurement of GB composition by Auger electron

DD FORM 1 JAN 73 1473 EDITION OF 1 NOV 65 IS OBSOLETE

Unclassified

SECURITY CLASSIFICATION OF THIS PAGE (When Data Entered)

spectroscopy (AES) and 2) attempt to relate changes in GB composition (i.e., Mg or Zn segregation) to changes in SCC susceptibility.

Three methods of inducing intergranular fracture were evaluated: 1) fracture at near-liquid nitrogen temperatures, 2) fracture after pre-exposure to liquid gallium, and 3) fracture after pre-exposure to water vapor-saturated air (WVSA). Fracture at near-liquid nitrogen temperatures was shown to be of a ductile intergranular nature and therefore, fracture was not on the exact GB surface. Fracture after pre-exposure to liquid gallium proceeded on the actual GB surface, but the Ga reacted with the fracture surface in a manner that changed its local chemistry. Fracture after pre-exposure to WVSA (i.e., hydrogen pre-exposure embrittlement: H-PEE) is brittle intergranular and no reaction occurred with the fracture surface, thereby allowing composition to be measured by AES.

The H-PEE fracture technique was then used to measure GB compositions for an alloy whose SCC susceptibility was varied by changing either solution heat-treatment temperature (SHT) or aging time. The SCC susceptibility as measured by plateau crack velocity or reciprocal time-to-failure was shown to decrease with both increasing SHT and increasing aging time. "Free-Mg," i.e., unbound in $MgZn_2$ precipitates, was present on all boundaries as shown by AES, but no correlation was observed between Mg concentration and changes in SCC susceptibility. Possible explanations from these results are discussed.

TABLE OF CONTENTS (Continued)

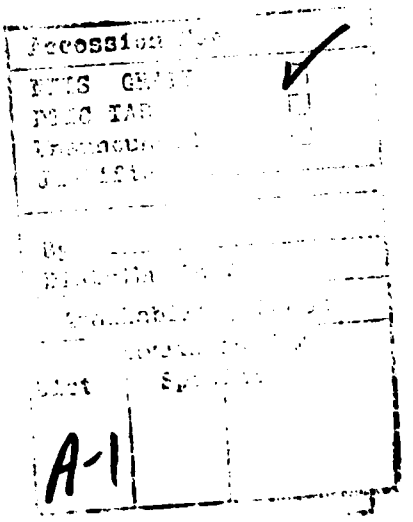

LIST OF FIGURES

LIST OF FIGURES (Continued)

LIST OF FIGURES (Continued)

Intergranular Fracture of Al-Zn-Mg Alloys in Embrittling Environments

by:

T.J. Langan and J.R. Pickens
MARTIN MARIETTA CORPORATION
Martin Marietta Laboratories
1450 South Rolling Road
Baltimore, Maryland 21227

I. INTRODUCTION

Many embrittlement phenomena are intergranular. This is particularly true in the case of Al-Zn-Mg alloys in which exfoliation corrosion is invariably intergranular, and hot shortness during metal working often occurs along grain boundaries. In addition, environmentally assisted cracking (EAC) phenomena such as stress-corrosion cracking (SCC), hydrogen embrittlement (HE), and liquid-metal embrittlement (LME) are usually intergranular.

Intergranular embrittlement phenomena can be greatly affected by grain boundary (GB) segregation. For example, the presence of GB precipitates is almost always a necessary condition for SCC, and segregation of Group I metal atoms can lead to the formation of low-melting point eutectic phases which can cause hot shortness. Consequently, measuring GB segregation is useful in studying the mechanisms by which embrittlement phenomena operate.

Several techniques have been used to study GB segregation in Al-Zn-Mg alloys. Doig, Edington, and their colleagues used electron energy loss spectroscopy (EELS) and X-ray microanalyses[1-5] on transmission electron microscope (TEM) thin foil specimens with grain boundaries oriented parallel to the electron beam. These techniques showed that solute concentration profiles vary greatly, depending on heat treatment and quenching rate. Concentration profiles across the precipitate-free zones (PFZs) and grain boundaries for a number of interrupted-quenched specimens showed higher solute concentration in the PFZ than in the grain interior.[1-4] In another study,[3] they showed magnesium segregation on the GB for a specimen that was fast-quenched and magnesium depletion for a slow-quenched specimen. In both cases, solute concentration on the actual GB was very difficult to determine because of the limited spatial resolution of these analytical electron microscopic techniques.

In an attempt to improve spatial resolution, Green and Montague,[6] Chen et al.,[7] Sun et al.,[8] and Viswanadham et al.[9] used Auger electron

spectroscopy (AES) to more carefully measure GB segregation on Al-Zn-Mg alloys by examining intergranular fractures made under ultra-high vacuum (UHV). This technique enables chemical analysis to be performed from ~3-6 atomic layers of the surface under investigation. Thus, if intergranular fracture could be induced on the actual boundaries, AES could be used to measure composition from a region much closer to the actual GB than would be possible using microanalytical techniques on GB profiles on thin foil specimens.

Green and coworkers[6-9] fractured Al-Zn-Mg alloys at liquid nitrogen temperatures under UHV, producing seemingly intergranular fractures and measured composition by AES on the specimen surfaces. The composition of the PFZ was determined by combining ion sputtering with AES. This technique enabled information to be obtained over an area of about 6-8 grain facets on the alloys investigated. They found that segregation of Mg atoms on the boundaries exceeded that which would be expected from the presence of the equilibrium $MgZn_2$ precipitates on the boundaries of Al-Zn-Mg alloys. They also found that the PFZ was solute-depleted. Consequently, they proposed that "free Mg," i.e., unbound in GB precipitates, exists on the boundaries of Al-Zn-Mg alloys. Additional evidence for the presence of this free Mg was also obtained using plasmon energy losses associated with Auger peaks.[8]

In recent work, using more advanced equipment than that used by Doig and Edington,[1-5] Malis and Chaturverdi[10] performed energy dispersive X-ray microanalysis on TEM specimens of an Al-8Mg* alloy. They also concluded that free Mg atoms segregate to the boundaries. However, a nominal 200-Å electron beam, passing through a 1000- to 3000-Å thick foil broadens to 300-400 Å, thus making it much larger than the boundary. In fact, Malis and Chaturverdi had to rely on a large sample space to show statistically that free Mg atoms were indeed on the boundaries.

---

* All compositions are given in wt%, unless stated otherwise. Thus, Al-8Mg is an aluminum alloy containing 8wt% Mg.

It is quite clear that AES offers tremendous possibilities for measuring segregation in the exact GB region, if in-situ intergranular fracture could be induced on the actual GB surface. In the present work, fracture in various embrittling environments was investigated to: 1) develop a technique that produces fracture on the GB surface, thereby enabling segregation to be measured, and 2) elucidate the nature of intergranular fracture in the Al-Zn-Mg alloy system.

II. MATERIALS

Three high-strength Al-Mg-Zn alloys were studied -- two high-purity model alloys and a commercial 7xxx alloy. Both model alloys, alloy G and alloy L, were chill-cast, homogenized, and hot rolled.

Alloy G is a high-purity Al-4.4Mg-3.7Zn alloy (Table 1) with no grain refiner, containing large equiaxed grains measuring ~170 μm. Specimens were solutionized at 475°C, ice water-quenched, and based on an aging study, aged for 100 min at 150°C to produce the peak-aged temper.

Alloy L is an Al-6.9Mg-2.9Zn-0.1Zr alloy (Table 1), where the 0.1Zr provides grain refinement. Its microstructure was partially recrystallized having equiaxed grains ~50μm in diameter and pancaked grains having a mean linear intercept of 155 x 78 x 29 μm in the longitudinal (L), long transverse (LT), and short transverse (ST) directions, respectively. Specimens were solutionized at 475°C followed by ice water quenching. Two different tempers were examined; peak-aged (20 h @ 121°C) and over-aged (300 h @ 121°C).

The commercial alloy studied was 7091-T6E192 (composition in Table 1). Alloy 7091 is a high-strength, rapidly solidified, powder metallurgy alloy, which was extruded into a 11.4 x 3.8 cm (4.5 x 1.5 in) rectangular bar. This alloy has an extremely fine grain size of 5 x 2 x 2 μm in the L, LT, and ST orientations, respectively.

High-purity gallium (i.e., 99.999) was used for the subsequently described LME experiments.

TABLE 1

Alloy Compositions

Alloy		Zn	Mg	Zr	Cu	Co	Impurities	Al
L	wt%	6.92	2.85	0.13	---	---	<0.01	Balance
	at%	3.00	3.30	0.03	---	---	---	Balance
G	wt%	4.40	3.70	---	---	---	<0.01	Balance
	at%	1.80	4.20	---	---	---	---	Balance
7091	wt%	6.50	2.60	---	1.55	0.44	---	Balance
	at%	2.64	2.83	---	0.70	0.20	---	Balance

III. EXPERIMENTAL PROCEDURES

Three in-situ fracture techniques were evaluated. The first involved fracture at near-liquid nitrogen temperatures. Specimens were placed in contact with a liquid nitrogen-cooled fracture unit in the Physical Electronics model 595 scanning Auger microprobe (SAM) at the National Science Foundation Facility at the University of Minnesota for 15-20 min. Joshi et al. [11] estimate that this method cools the specimen to about -135°C. The specimen was then fractured by impact and moved under the electron beam for analysis.

The second technique used liquid gallium pre-exposure embrittlement (Ga_L-PEE) to induce intergranular fracture. The embrittling procedure used was as follows:

- Each specimen is heated to ~35°C, which is slightly above the melting point of gallium (29.87°C).
- A ~0.01g droplet of Ga_L is placed on a warm scalpel blade, which is then used to scribe the specimen, thereby leaving gallium in the scribe mark.
- The specimen is then held at 35°C for about 1 h to allow the Ga to diffuse along the grain boundaries.
- The embrittled specimen is then placed in the UHV bell jar of the spectrometer, and moved into contact with the fracture stage, which is heated to 35°C.
- The specimen is then fractured by impact and is immediately moved under the electron beam for analysis.

The third technique induces fracture by hydrogen embrittlement by pre-exposing the specimens to moist air as follows:

- o Each specimen is placed in an autoclave in water vapor-saturated air (WVSA) at 100°C at a pressure of 1 atmosphere gauge (15 psig) for 8 to 24 h.

- o The specimen is then placed in the bell jar of the Auger unit without removing the oxide-hydroxide surface film.

- o The specimen is then impact fractured under UHV at room temperature and analyzed by AES.

The accelerating voltages used for the SAM were 5 and 15 kV. Area selection was carried out using the electron imaging capabilities of the microprobe. A probe size from 1000-2000 A was used for analysis. The scanning mode of the SAM permitted high-resolution elemental mapping of the fracture surfaces. Survey scans from 24-1550 eV were used to determine changes in Mg, Al, and Zn concentrations for the various specimens. For these surveys, the data were collected in the N(E) mode and later differentiated to give dN(E)/dE surveys from which peak-to-peak heights were determined. In most cases, surveys from two point locations on each specimen surface were recorded simultaneously.

Although gallium pre-exposure embrittlement (Ga_L-PEE) and liquid-nitrogen-induced fracture surfaces were also analyzed using a "static" Auger, use of this system was limited because of its relatively coarse probe size (300 μm) and lack of electron imaging capability. An accelerating voltage of 5 kV was used for all "static" Auger measurements. All surveys were electronically differentiated and recorded as dN(E)/dE spectra. Multiplexing with and without sputtering was also performed using this system. Vacuum pressures generally ranged from 3×10^{-8} to 1×10^{-9} torr.

Semi-quantitative elemental ratios (e.g., Mg/Al and Zn/Al) were calculated for fracture surface compositions using peak-to-peak heights from differentiated spectra from both "static" AES and SAM. Differences in elemental sensitivities were corrected for by using published sensitivity factors.[12] High-resolution scanning electron microscopy was performed on selected specimens in a JEOL 100-CX to determine whether the fracture was intergranular.

IV. RESULTS

A. FRACTURE AT NEAR-LIQUID NITROGEN TEMPERATURES

Fracture at near-liquid nitrogen temperatures appears intergranular at low magnification as seen on a peak-aged alloy G fracture (Fig. 1a), with no resolvable evidence of ductile fracture (e.g., no dimples). However, at higher magnification, microdimples become apparent (Fig. 1b). Consequently, fracture at near-liquid nitrogen temperatures is ductile intergranular, most likely proceeding in the PFZ. For comparison, Fig. 2 shows the surface of a peak-aged alloy G specimen fractured at room temperature. The fracture is somewhat intergranular, but large dimples can be seen at high magnification. The PFZ size for alloy G in the peak-aged temper is about 0.3 μm. Comparing the dimple sizes between Fig. 1b and 2b, we see that dimples produced after fracture at near-liquid nitrogen temperature are closer in depth to the PFZ size than those formed by room temperature. Thus, room temperature fracture is more ductile in appearance and is less intergranular than that fractured at near-liquid nitrogen temperatures.

The effect of the atmosphere in the bell jar at UHV on liquid nitrog . fracture surfaces was determined by multiplexing without sputtering. No changes in the Mg/Al ratio were observed with increasing time after fracture. Thus, at the vacuum levels obtained (i.e., 1 to 2×10^{-9} torr), surface composition did not depend on time after fracture. This result will be shown to contrast with that from fracture surfaces obtained after pre-exposure to liquid gallium.

B. FRACTURE AFTER PRE-EXPOSURE TO LIQUID GALLIUM

Liquid gallium has been shown to be a severe intergranular embrittler of aluminum alloys[13-18]. SEM micrographs of a Ga_L-PEE fracture surface are shown in Fig. 3. The low-magnification micrograph (Fig. 3a) has the same

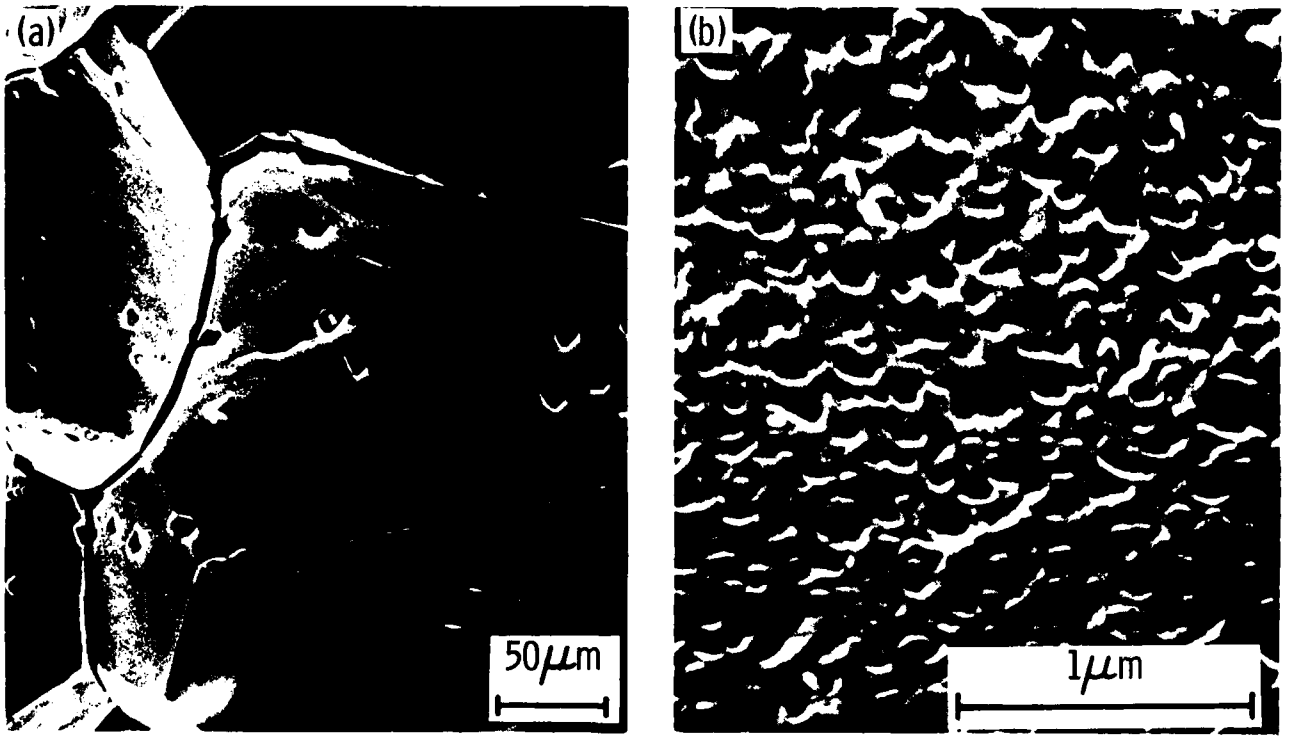

Figure 1. SEM micrographs from fracture of alloy G at near-liquid nitrogen temperatures showing a) intergranular facets and b) microdimples in facets.

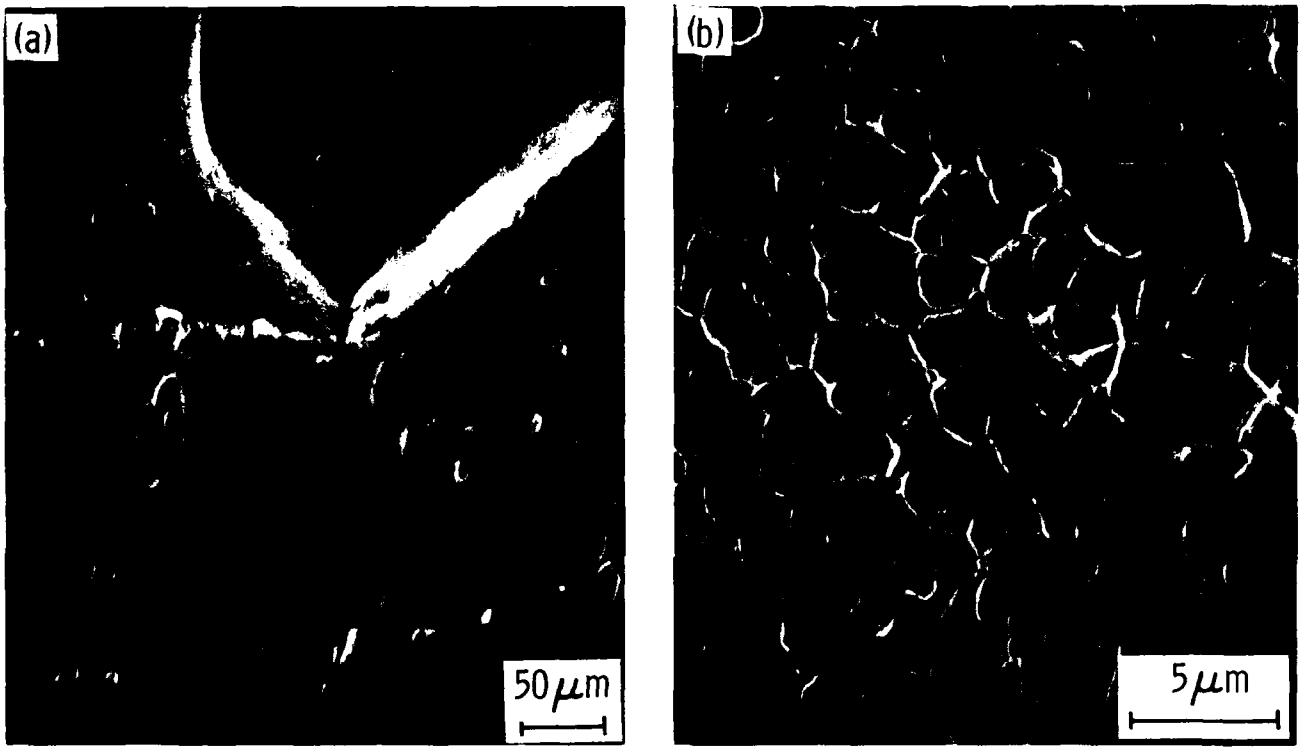

Figure 2. Low-and high-magnification SEM micrographs from fracture of alloy G at room temperature using no embrittlement technique.

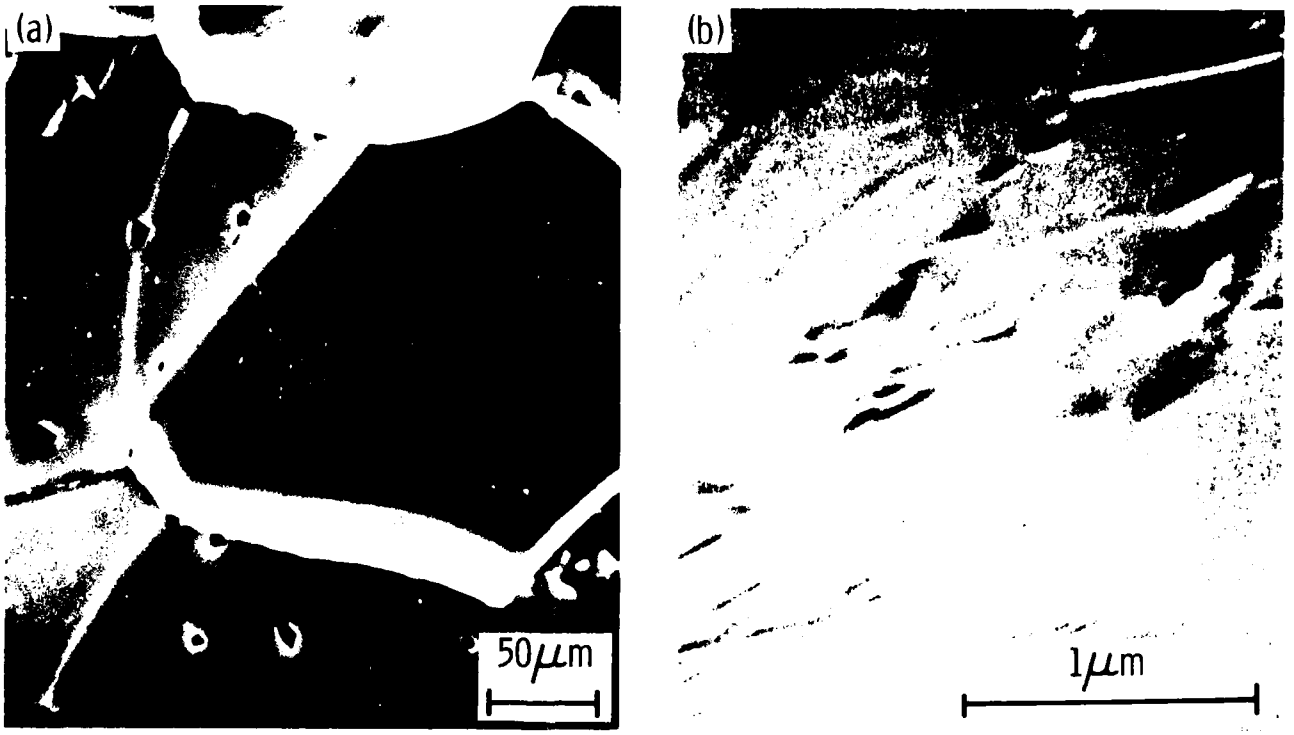

Figure 3. Low and high-magnification SEM micrographs from fracture in alloy G after exposure to liquid gallium a) intergranular facets, and b) no microdimples present.

intergranular appearance as Figure 1a, but the high-magnification micrograph (Fig. 3b) shows none of the microdimpling observed on the near-liquid nitrogen fracture surface (Fig. 1b). To the limit of resolution of the SEM, the fracture appears completely brittle and on the actual grain boundary.

The fracture surfaces are covered with a thin layer of Ga_L and are very reactive, as evidenced by the following observations. Figure 4 shows SEM micrographs from an alloy G specimen that was pre-exposed to liquid gallium, fractured in ambient (i.e., moisture-containing) air, and placed in the vacuum chamber of the SEM 10 min after fracture. The surface of the specimen is covered by a thin brittle film, which cracked as the result of hydration or amalgamation reactions occurring under it. An AES survey scan of the surface showed relatively little gallium but high concentrations of Mg and Al oxides (Fig. 4). Laboratory air is obviously a much more aggressive environment than the UHV atmosphere in the spectrometer, but this experiment illustrates the extreme reactivity of the surface. Changes observed on the surfaces of specimens fractured under UHV are more subtle, but nevertheless are present as discussed below.

Auger depth profiles started 2 and 19 minutes after fracture show that shortly after fracture of a Ga_L-PEE alloy G specimen, the surface is covered by a very thin gallium layer (Fig. 5a). The depth profile that began 19 minutes after fracture shows that a thin Mg-Al oxide film forms on top of the gallium layer (Fig. 5b). These profiles along with the micrographs and survey scans from fracture in laboratory air suggest that the Mg and Al diffuse through the gallium layer and form a thin oxide film on its surface, thus changing the surface composition as measured by AES.

The change in the relative magnesium concentration associated with surface oxidation is shown by plotting the Mg/Al peak-to-peak ratio, after adjusting for differences in elemental sensitivities, with increasing time after fracture. Ultra-fine grained alloy 7091 was used for this experiment, and the 300-μm electron beam of the Auger spectrometer encompassed many

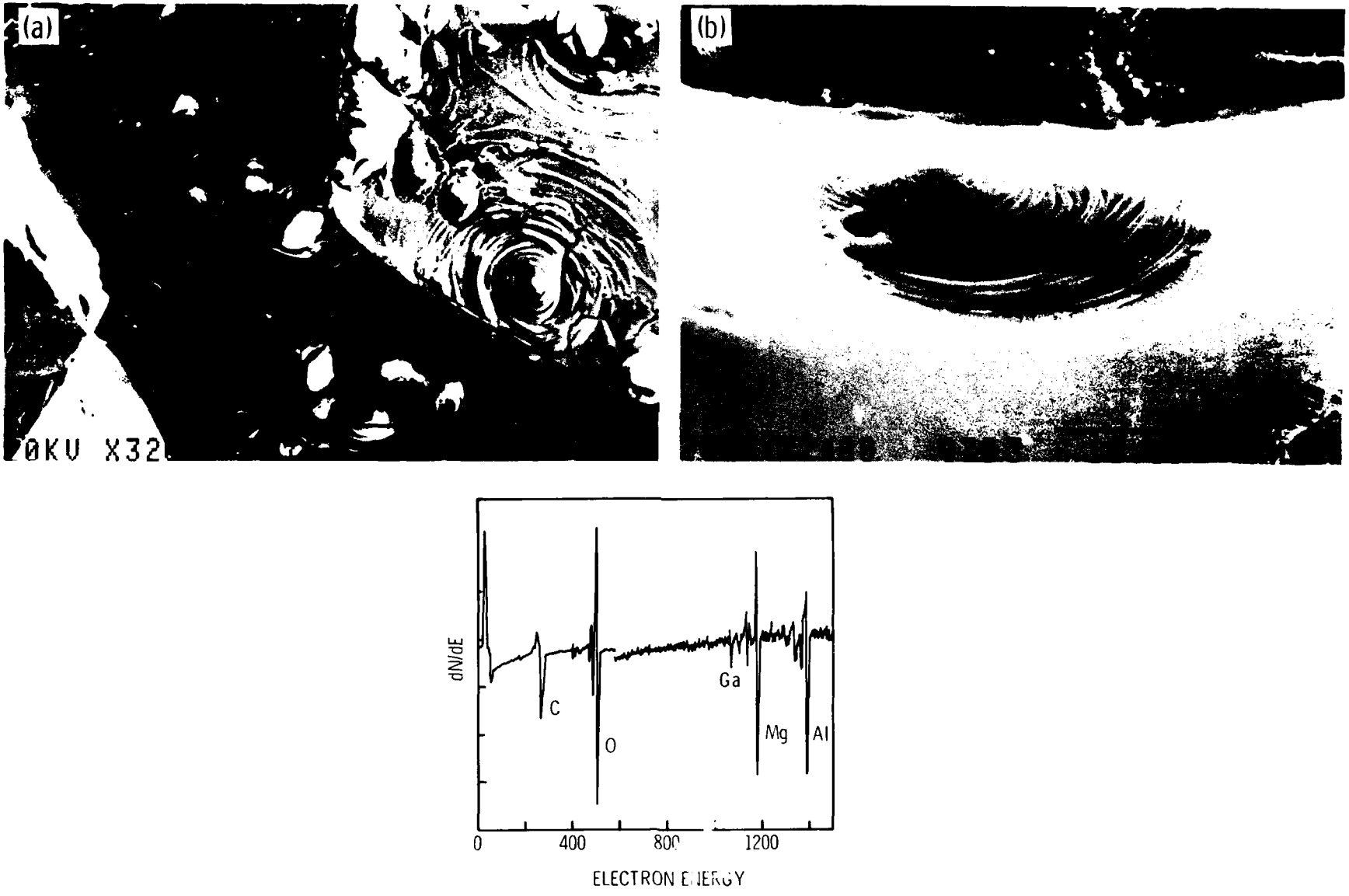

Figure 4. Low-(a) and high-(b) magnification SEM micrographs showing liquid gallium-induced fracture of alloy G after exposure to moist air. Insert is an Auger survey scan from this surface.

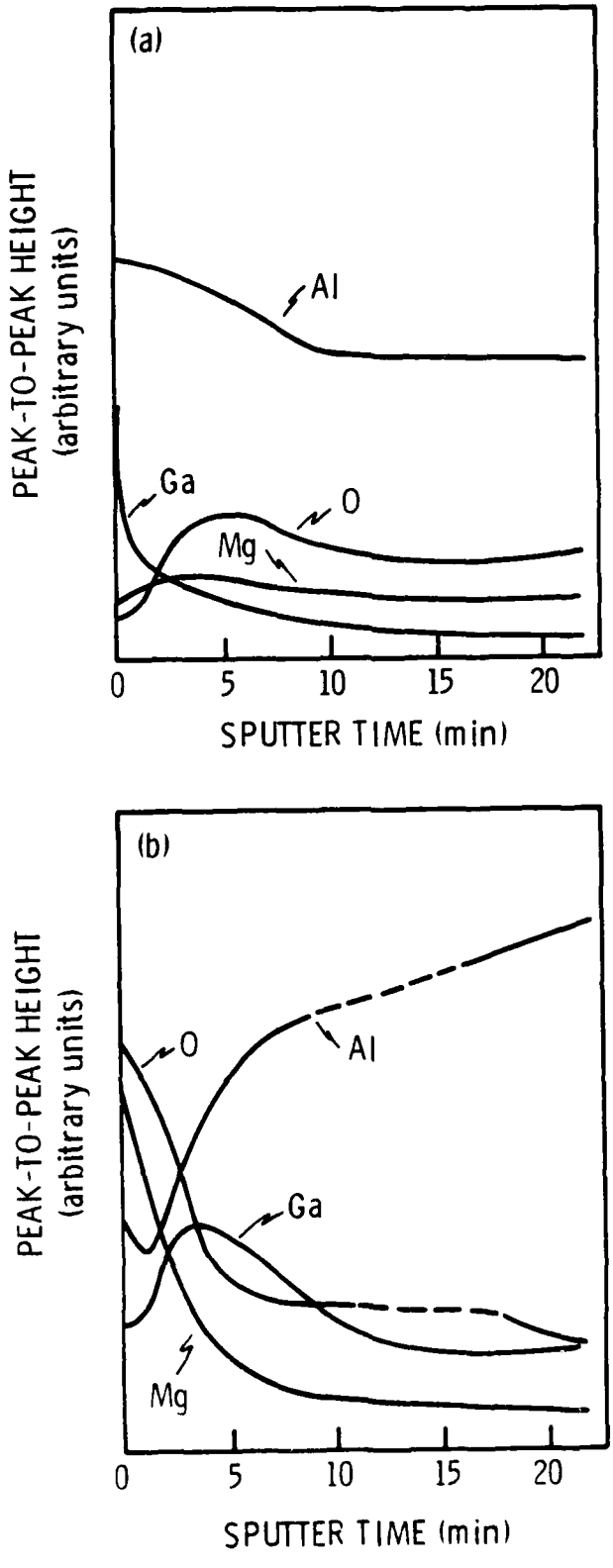

Figure 5. Two Auger depth profiles from fracture of alloy G after pre-exposure to Ga_L a) profiling started 2 min after fracture and b) started 19 min after fracture.

grains. Fracture was performed at two vacuum pressures and the change in the Mg/Al ratio was plotted (Fig. 6) along with the associated aluminum KLL Auger transition. The Mg/Al ratio increases with time under the electron beam and furthermore the measured values of Mg/Al are higher at the poorer vacuum pressures. It should also be noted that as the Mg/Al ratio increases, the line shape of the aluminum KLL Auger transition shows increasing oxide character.

The reactivity of the fracture surface and the mobility of the various elements was assessed by multiplexing without ion sputtering. This was done by recording the changes in peak-to-peak heights with increasing time after fracture. Magnesium and oxygen increase linearly with time (Fig. 7); aluminum remains nearly unchanged and the gallium decreases slightly.

Changes in elemental distributions with time after fracture were also determined by Auger surface mapping. A secondary electron image from a Ga_L-PEE alloy L fracture surface is shown in Fig. 8a. Bright spots on the fracture surface indicate gross changes in the surface electron scattering properties as a result of changes in topography or composition. Mapping immediately after fracture shows gallium present on the entire surface (Fig. 8b) with areas of higher concentration on the bright spots. The magnesium map taken at about the same time shows no magnesium present on the surface (Fig. 8c). Fifteen minutes after fracture, a high concentration of Mg (Fig. 8d) is seen on the bright spots with oxygen concentrations in close association (Fig. 8e). Mapping after 15 minutes of sputtering at about 50Å/min shows gallium present (Fig. 8f) on most of the surface with higher concentrations on the bright spots. In addition, aluminum is present everywhere on the surface except on the bright spots (Fig. 8g) and magnesium is present only on the spots (Fig. 8h). This shows that the surface changes shown in Figs. 4-8 occur in very localized regions on the fracture surface that are closely associated with the bright spots.

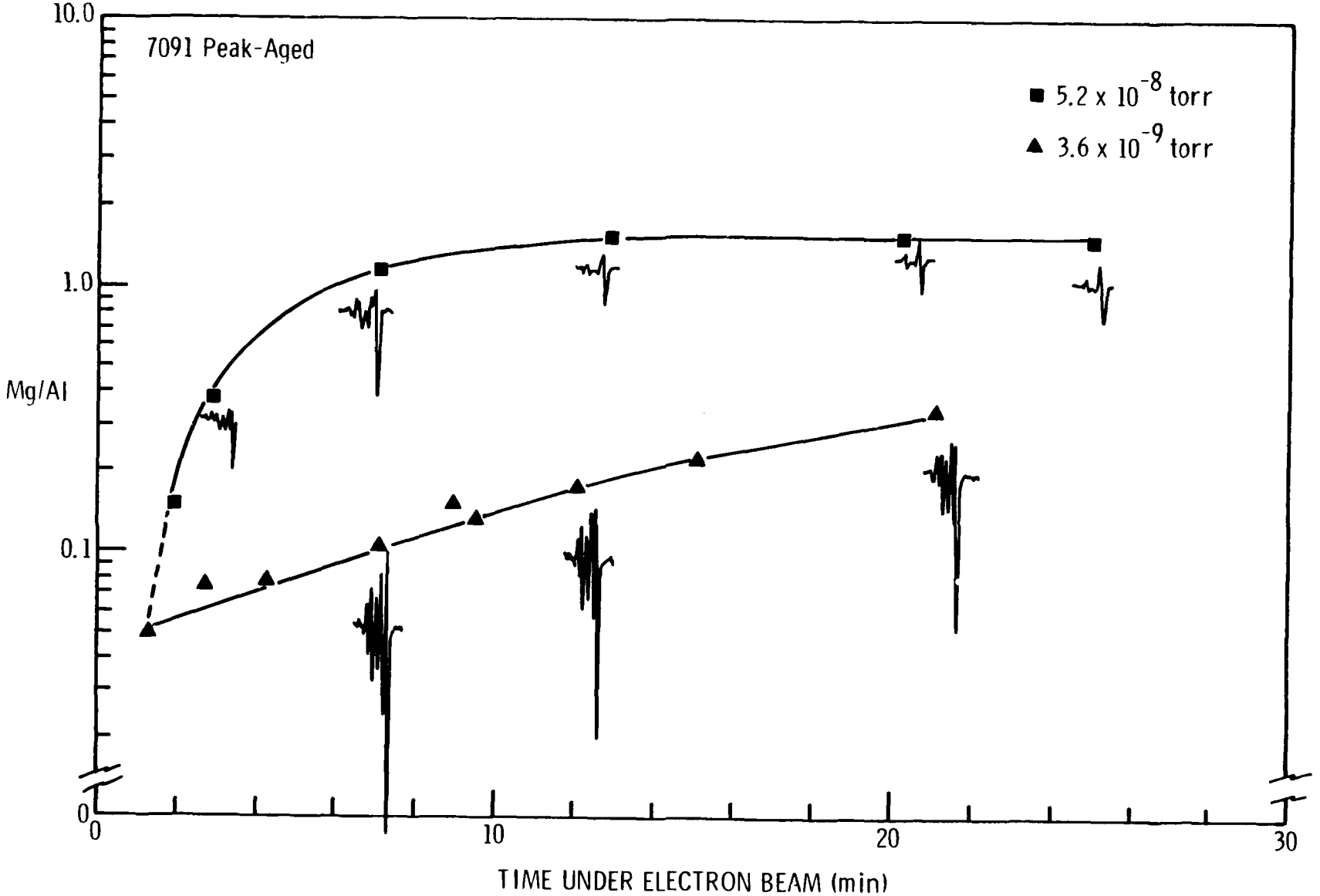

Figure 6. Change in Mg/Al with time after fracture for 7091. Aluminum K_{LL} Auger transition shape shown at various points along line.

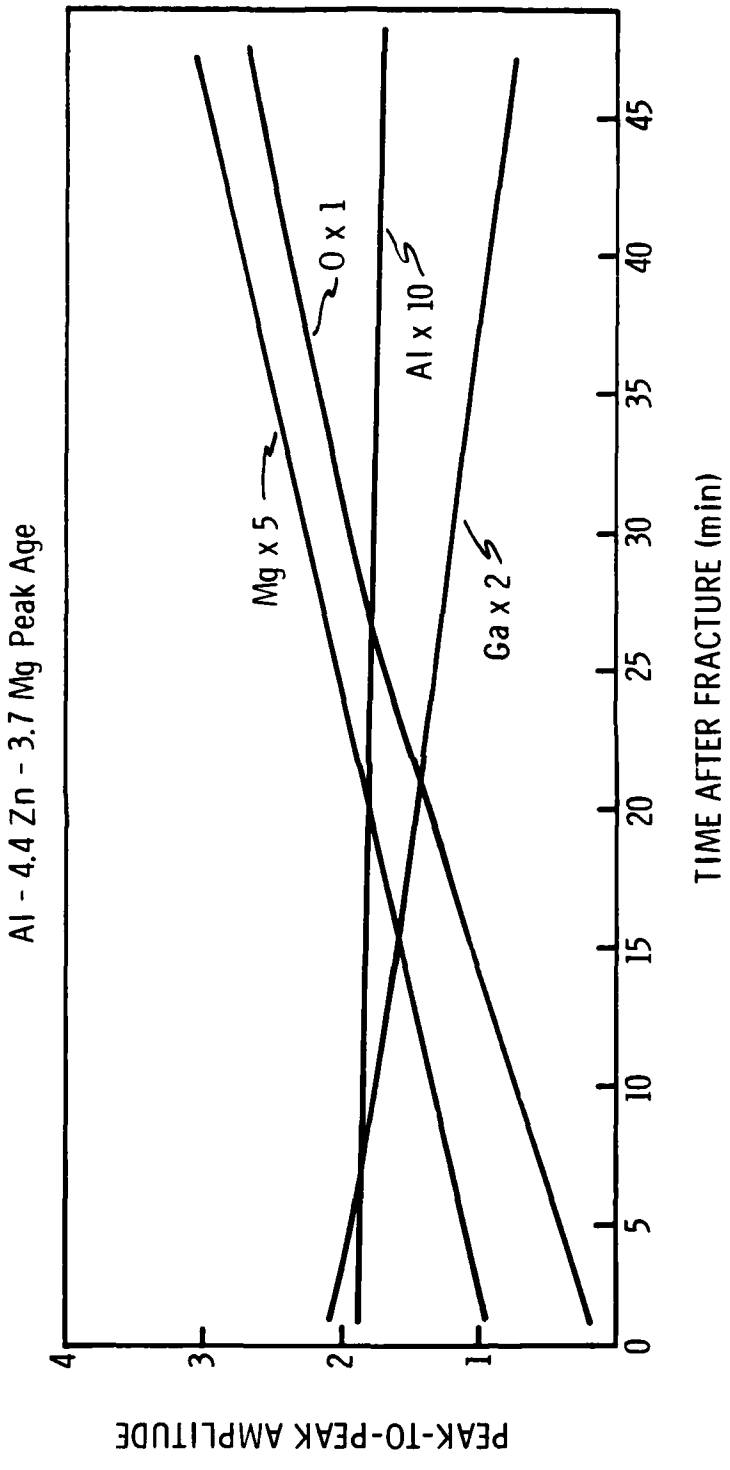

Figure 7. Multiplex plot showing changes in peak-to-peak heights for Mg, O, Al, and Ga with time after fracture. Alloy G specimen was pre-exposed to liquid gallium.

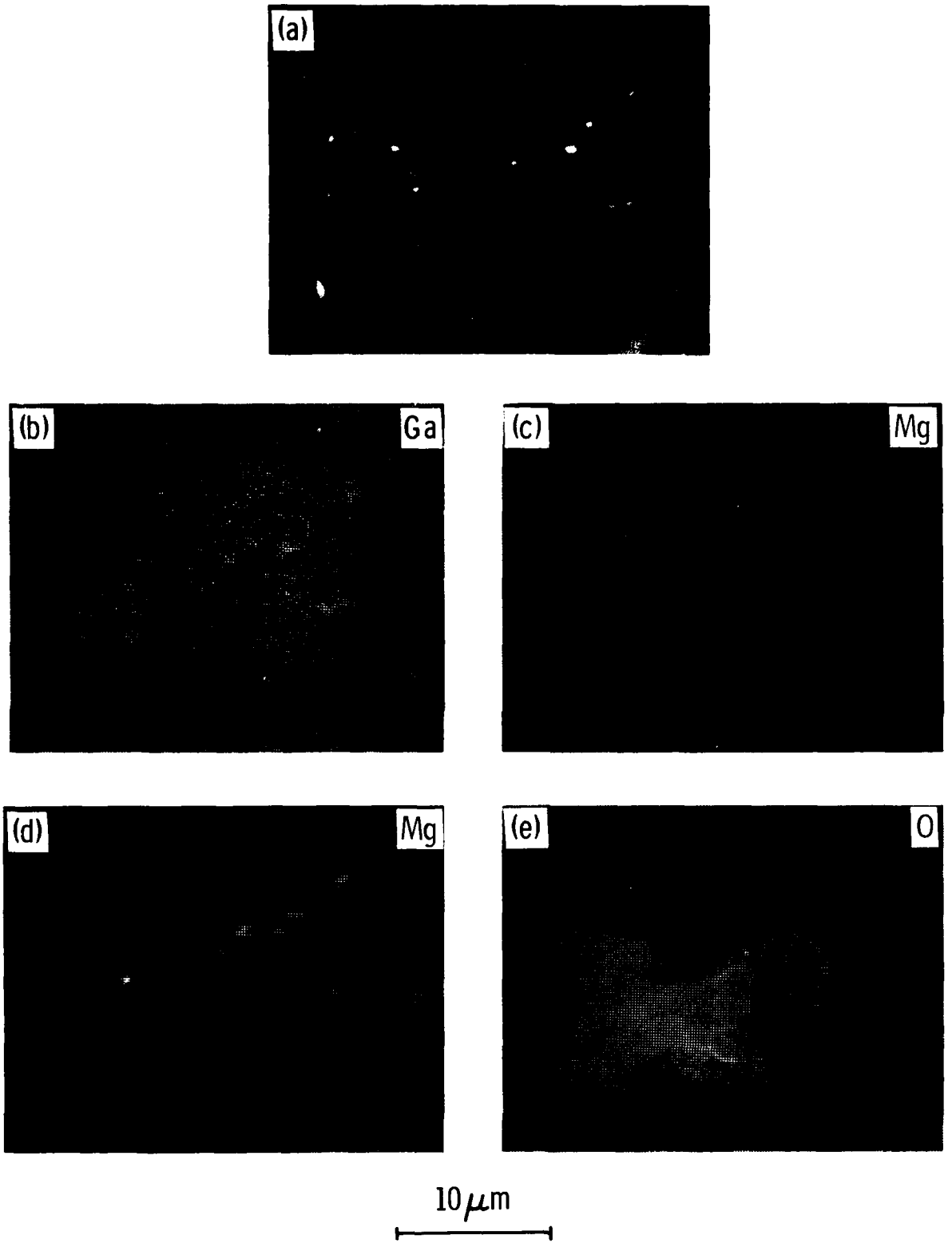

Figure 8. Elemental mapping on alloy L fractured after exposure to Ga_L: a) electron image at fracture surface, b-c) Ga and Mg maps immediately after fracture, d-e) Mg and O mapped 15 min after fracture, and f-h) Ga, Al, and Mg maps after sputtering ~ 50 Å.

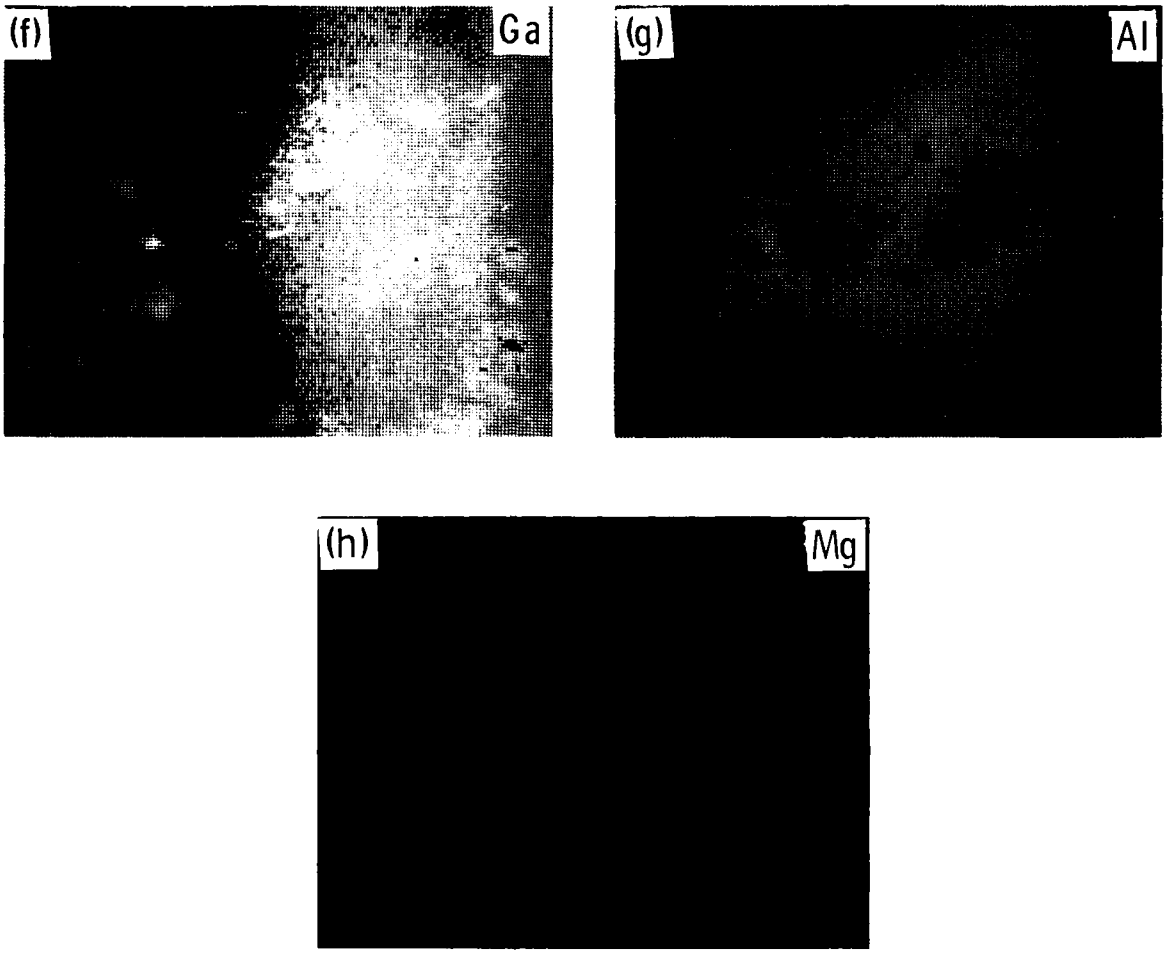

Figure 8. Continued from previous page.

Changes in composition with depth at various locations on a Ga_L-PEE alloy L fracture surface were determined by depth profiling on eight points selected from an electron image of the fracture surface (Fig. 9a). Profiles from two representative points are shown in Fig. 9b and c. These were carried out simultaneously starting about 15 min after fracture. Point #1 is from a bright spot and point #5 is from the dark area between the spots. The relative surface concentrations of gallium and oxygen were very high from both points. The surface composition at point #1 also has a high concentration of magnesium (Fig. 9b). After about 1 min of sputtering, the oxygen layer is gone and the magnesium is near its bulk level. The aluminum concentration increases steadily until it begins to level off after about 7 min of sputtering. Gallium is present at high concentrations all the way through the profile, reaching its peak value just after the oxygen layer is gone. As sputtering begins on point #5 (Fig. 9c) the aluminum concentration increases as the gallium and oxygen concentrations drop off. After 1 min of sputtering (~36 Å), the gallium and oxygen concentrations level off at what appears to be their bulk values. No magnesium is present on the surface and little, if any, appears upon sputtering into the material. These depth profiles show that the bright spots have a different composition than the surrounding surface and that they probably are globules of gallium.

C. FRACTURE AFTER HYDROGEN PRE-EXPOSURE EMBRITTLEMENT (H-PEE)

Exposing specimens to liquid or gaseous H_2O can charge hydrogen into aluminum alloys, i.e., hydrogen pre-exposure embrittlement (H-PEE), which renders the alloy susceptible to intergranular fracture.[18-22] Precharged specimens of alloy G produced ductile intergranular fractures (Fig. 10a); at high magnifications, extensive microdimpling was present (Fig. 10b). The fracture surfaces of alloy L specimens that were exposed to WVSA at 1 atmosphere gauge for 24 h and fractured under UHV are clearly intergranular (Fig. 10c). Some regions show signs of ductile fracture, but most facets

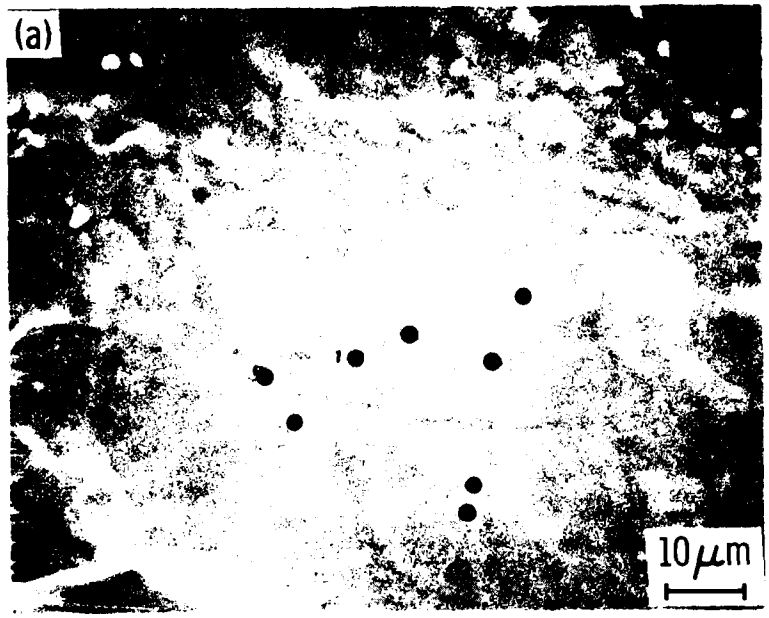

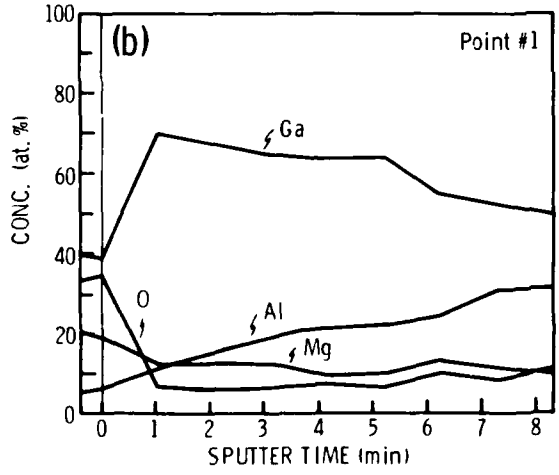

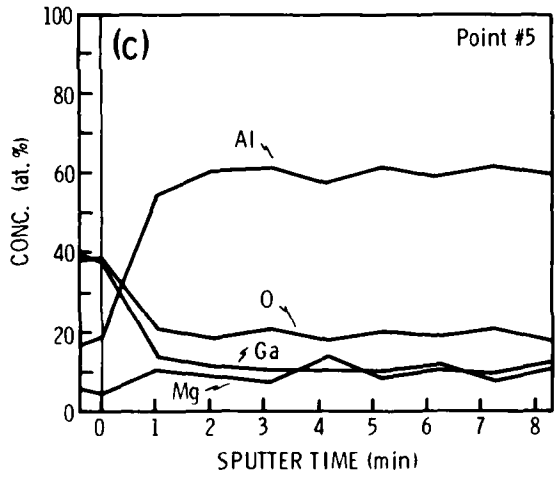

Figure 9. Alloy L fracture after Ga_L pre-exposure showing a) bright spots (e.g., #1), whose depth profile (sputtered at 150Å/min) b) reveals that the spots are higher in Ga and Mg than the c) area between them (e.g., #5).

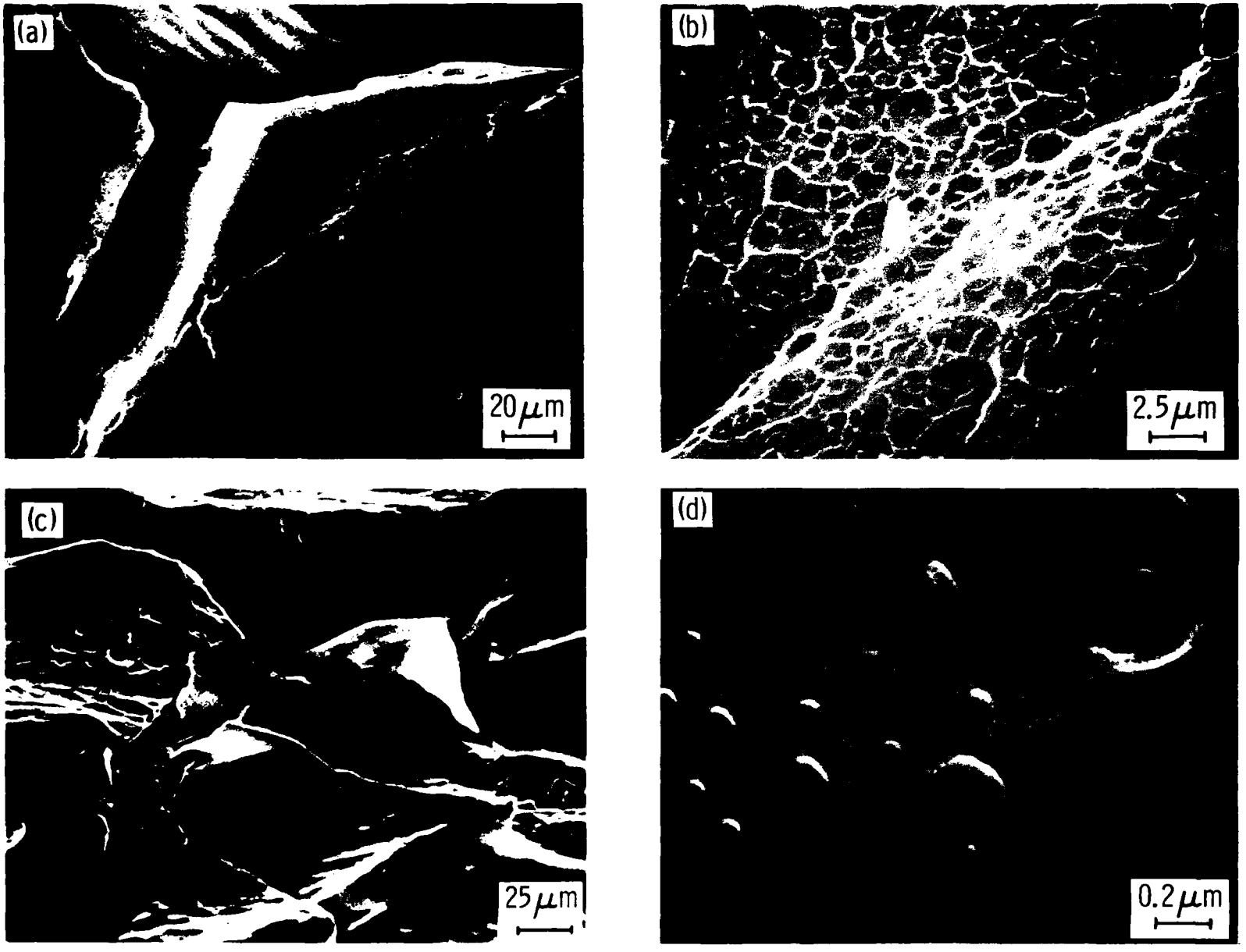

Figure 10. SEM micrographs of fractures induced by pre-exposure to WVSA at 100°C showing: a) intergranular facets in equiaxed grained alloy G, b) dimples on facets in (a), c) intergranular facets in pancake-grained alloy L, and d) GB precipitates visible but no dimples on facets in (c).

appear featureless at lower magnification. At high magnification, voids are present resulting from GB precipitate/matrix decohesion (Fig. 10d), but microdimpling was not observed. The intergranular nature of the fracture is further illustrated by a cross-sectional micrograph showing the fracture surface from a H-PEE Auger fracture specimen (figure in ref. 23).

Alloy L was extremely susceptible to H-PEE in the peak-aged temper. Precharged specimens of the normally ductile alloy L could be broken by hand in much the same fashion as a glass rod of similar dimensions. Susceptibility to H-PEE was also shown for alloy L in the as-quenched and overaged tempers, although some microdimpling was observed in the latter temper.

The high susceptibility to H-PEE of alloy L apparently eliminated any problems associated with strain rate sensitivity of fracture. TEM micrographs similar to those by Christodoulou and Flower[24] and Scamans[25] show hydrogen-bubbles present on the grain boundaries of both alloys G and L (Fig. 11), indicating that high concentrations of hydrogen are present there. With hydrogen clearly present on the GBs of alloy G, it is not immediately obvious why the fracture was ductile (Fig. 11).

The reactivity of the H-PEE fracture surface was measured using the same approach as for the Ga_L-PEE and liquid nitrogen-induced fracture surfaces. Relative atomic concentrations were recorded as a function of time after fracture. Aluminum, zinc, magnesium, and oxygen showed no changes with time after fracture at vacuum pressures around 2-3 x 10^{-9} torr.

It is apparent that changes in surface composition with time after fracture under UHV are much slower for H-PEE and fracture induced at near-liquid nitrogen temperature than for Ga_L-induced fractures: no change in Mg/Al with time was observed in the first two cases, but a rapid change was observed in the third. This indicates that surface oxidation under UHV is not rapid enough to change the surface composition on H-PEE and near-liquid nitrogen fractures as measured by AES. This eliminates concerns about the validity of data collected at different times after fracture from H-PEE and liquid nitrogen-induced fracture surfaces.

Figure 11. TEM micrograph showing hydrogen bubbles present on grain boundary of alloy G after pre-exposure to WVSA at 100°C.

V. DISCUSSION

A. FRACTURE AT NEAR-LIQUID NITROGEN TEMPERATURES

Impact fracture at both room and near-liquid nitrogen temperatures is ductile intergranular, as shown by the fracture surface micrographs (Figs. 1 and 2). Although both fractures have intergranular facets covered with microdimples, dimple size differs. Recently, Thompson[26] has related dimple size to the macroscopic ductility of a material and found that ductility increases with increasing dimple size. A fracture at near-liquid nitrogen temperatures has a finer dimple size than that observed for room temperature fractures, so the former fracture is likely closer to the actual grain boundary and probably more brittle. This decrease in ductility at cryogenic temperatures is not typically found in face-centered cubic (FCC) metals, but has been observed in high-strength, highly alloyed 7xxx alloys.[27-29]

Christian and Watson[27] proposed that a decrease in ductility at cryogenic temperatures results from an increase in fracture initiation at GB precipitates and intermetallic inclusions. The three 7xxx alloys studied have a high volume fraction of precipitates; thus, this is a possible explanation for the decrease in ductility observed at near-liquid nitrogen temperatures. Kaufman and Wanderer[28] observed a correlation between temper and loss of ductility at cryogenic temperatures, with peak-aged (i.e., T6) 7075 being slightly more brittle than overaged (i.e., T73) 7075. Therefore, if fracture at near-liquid nitrogen temperature is to be used to expose boundaries for segregation measurements, care should be taken when comparing segregation measurements from two different tempers, because fracture in the peak-aged temper may be closer to the actual grain boundary.

Although liquid nitrogen temperatures tend to decrease the ductility of 7xxx series alloys, the fracture path still proceeds off the actual boundary surface; through the PFZ. Therefore, chemical analysis from surfaces fractured at near-liquid nitrogen temperatures may not truly represent the GB composition.

B. FRACTURE AFTER PRE-EXPOSURE TO LIQUID GALLIUM

Fracture after exposure to liquid gallium is completely brittle intergranular with no dimples visible on any GB facets. This result is in agreement with results of Preece and Westwood,[13] who observed no measurable ductility in Ga_L-induced fracture studies on polycrystalline aluminum alloys. Thus, fracture after exposure to liquid gallium is completely on the GB surface, which is the region of interest in segregation studies. However, as shown by Figs. 5 to 11, the gallium reacts with aluminum, magnesium, and oxygen, thereby changing their relative compositions on the exposed surface.

This reaction results in the surface enrichment of Mg for all three alloys (Figs. 6-8). This movement occurs in a very small volume of material relative to the bulk, but the high surface sensitivity of AES allows a large change in composition to be measured. Upon or immediately following fracture, the surface is covered with a thin layer of gallium (Fig. 8b). With time, it is possible that magnesium and aluminum from the fracture surface of the alloy are dissolved into this gallium layer, diffuse through the layer, and are oxidized on its surface. The Mg enrichment of the resulting oxide film could result from one or more of three possible factors: 1) magnesium is present on the fracture surface in an active state which goes into solution with the liquid gallium more readily than the aluminum, 2) magnesium has a higher diffusion rate in liquid gallium than does aluminum, and 3) magnesium has a higher affinity for oxygen than does gallium or aluminum.

It is unclear whether the free-Mg[6-9,23] on the intergranular fracture surface diffuses through the Ga layer, or the Ga diffuses through the free-Mg

layer and into the bulk aluminum alloy, thereby allowing the free-Mg to reside on the free surface. Hunter and Scamans[30] showed that Ga on fresh aluminum surfaces diffuses into the bulk of the alloy at room temperature. However, their observation was made on an alloy that did not have a thin free-Mg layer and thus, may not have implications for the issue at hand.

Gallium and magnesium have low mutual solubilities,[31] so, at first glance, it is suprising that the Mg layer forms so rapidly on the Ga_L-PEE fracture surface. Perhaps the mutual solubilities of Ga and Mg are much higher in thin, surface-active films.

It is surprising that the Mg oxidizes much more rapidly on the Ga-PEE than the H-PEE fracture surface. We suspect that the Mg atoms in the somewhat continuous free-Mg film that is exposed by H-PEE-induced fracture would be less active than the individual Mg atoms exposed to the UHV atmosphere by diffusing through the Ga. That is, each Mg atom reaching the surface would have fewer neighbors and likely have a greater affinity for oxygen. This argument obviously points towards Mg atoms diffusing through the Ga, rather than the reverse.

Elemental mapping of the fracture surfaces shows that the magnesium movement occurs in highly localized regions associated with bright spots shown on secondary electron images. These regions appear to serve as short-circuit diffusion paths through which the magnesium movement is highest, as evidenced by the rapid changes in magnesium and oxygen concentrations on the bright spots with increasing time after fracture.

The spots are most likely globules of gallium. It is curious that the increase in concentration of Mg on these spots is more rapid than in regions off the spots, where the Ga layer is not as thick. Perhaps local concentrations of Mg under the spots are higher, due to interactions between the gallium, GB free-Mg, and GB $MgZn_2$ particles occurring just after fracture. It is unfortunate that practical considerations prevented sputtering all the way through the globules to determine the composition beneath them.

From these results, we conclude that exposure to liquid gallium produces fracture on the actual GB surface as desired, but that localized reactions change the surface composition, making accurate measurement of GB segregation extremely difficult.

C. FRACTURE AFTER HYDROGEN PRE-EXPOSURE EMBRITTLEMENT

In order to induce intergranular failure by H-PEE on the actual GB surface, the alloy must be susceptible to HE, and if in-situ fracture is to be induced by impact, this susceptibility must not be greatly diminished at high strain rates. Alloy L in the peak-aged temper apparently satisfies both of these requirements, as evidenced by the dimple-free surface fractures resulting from H-PEE. The dependence of HE susceptibility on strain rate has been shown to vary greatly with alloy composition. For example, Scamans et al.,[20] in slow strain rate tests on H-PEE specimens, showed that model alloys similar in composition to alloy L show very little, if any, dependence of ductility on strain rate.

On the other hand, alloys having lower solute content (i.e., %Zn + %Mg) were not embrittled after pre-exposure when tested at high strain rates.[20] Thus, alloy G has a lower solute content than alloy L, and apparently is less susceptible to HE. At the relatively high strain rates induced by impact, the alloy is not sufficiently susceptible to be embrittled on the actual boundary, and fracture proceeds through the relatively weak PFZ. This occurred despite the high concentration of hydrogen on the boundaries, as evidenced by the bubbles shown in Fig. 11.

Some dimples were observed for alloy L in the overaged temper indicating that it is not as susceptible to H-PEE in this temper as it is in the peak-age temper. This result is in agreement with the greater SCC susceptibility in the peak-aged than over-aged temper, since SCC in Al-Zn-Mg alloys has recently been shown to proceed <u>mostly</u> by hydrogen embrittlement.[32]

VI. CONCLUSIONS

For Al-Zn-Mg alloys:

- Fracture at near-liquid nitrogen temperatures is not completely on the GB surface, but also occurs through the PFZ, as evidenced by microdimples. Surface science analysis of the fracture surface may not give the composition of the actual GB.

- Fractures induced by pre-exposure to liquid gallium occur on the actual GB surface, as evidenced by the absence of dimples on the fracture surface at a resolution limit of 30 Å. However, the Ga alters the surface chemistry of the GB by changing the Mg/Al ratio. In addition, its presence on the fracture surface makes accurate measurement of Zn concentration difficult because of the similarity in Auger electron energies of the major Ga and Zn peaks.

- Fracture induced by pre-exposure to hydrogen-forming environments can be on the actual GB surface. For example, no dimples were observed in most regions of the fracture surface of an Al-6.9Zn-2.9Mg-0.1Zr alloy at a resolution limit of 30 Å. This method of inducing in-situ fracture enables investigation of an unaltered GB surface.

VII. ACKNOWLEDGEMENTS

The authors are grateful for the electron microscopy assistance and advice provided by Dr. L. Christodoulou during the early stage of this research. The technical assistance and discussions with Mr. H. Erskin and Drs. A. Taylor and G.T.K. Swami at National Science Foundation's surface analysis center at the University of Minnesota were essential to this work. We would also like to thank Drs. G.M. Scamans, J.D. Venables, and A. Joshi for their comments on the manuscript. Most of all, we appreciate the unwavering support of Contract Monitor Dr. P. Clarkin.

This work was supported by the Office of Naval Research under Contract No. N00014-84-C-380.

VIII. REFERENCES

1. P. Doig, J.W. Edington, and G. Hibbert, "Measurement of Mg supersaturation within precipitate-free zones in Al-Zn-Mg alloys," Philos. Mag., 28, 971 (1973).

2. P. Doig, J.W. Edington, and M.H. Jacobs, "Microanalysis across grain boundaries in aluminum alloys," Philos. Mag., 31, 285 (1975).

3. P. Doig and J.W. Edington, "Stress-corrosion susceptibility of as-quenched Al-5.9wt%Zn-3.2wt%Mg alloy," Br. Corros. J. (Quarterly) 9 (4) (1974)

4. P. Doig and J.W. Edington, "Influence of precipitate free zones on the stress corrosion susceptibility of a ternary Al-5.9wt%Zn-3.2wt%Mg alloy," Corrosion-NACE, 31 (10), 347 (1975).

5. P. Doig, P.E.S. Flewitt, and J.W. Edington, "The stress-corrosion susceptibility of 7075 Al-Zn-Mg-Cu alloys tempered from T6 to an overaged T7X," Corrosion-NACE, 33 (6), 217 (1977).

6. J.A.S. Green, and W.G. Montague, "Observation on the stress corrosion cracking of an Al-5%Zn-2.5%Mg ternary and various quarternary alloys," Corrosion, 31 (6), 209 (1975),

7. J.M. Chen, T.S. Sun, R.K. Viswanadham, and J.A.S. Green, "Grain boundary segregation of an Al-Zn-Mg ternary alloy," Metall. Trans. A, 8A, (1935) (1977).

8. T.S. Sun, J.M. Chen, R.K. Viswanadham, and J.A.S. Green, "Plasmon-loss satellites in Auger spectra of alloy surfaces," Appl. Phys. Lett., 31 (9), 580 (1977).

9. R.K. Viswanadham, T.S. Sun, and J.A.S. Green, "Grain boundary segregation in Al-Zn-Mg Alloys - Implications to stress-corrosion cracking," Metall. Trans. A., 11A, 85 (1980).

10. T. Malis and M.C. Chaturverdi, "Grain-boundary segregation in an Al-8wt%Mg alloy," J. Mater. Sci., 17, 1479 (1982).

11. A. Joshi, C.R. Shastry, and M. Levy, "Effect of heat treatment on solute concentration at grain boundaries in 7075 aluminum alloy," Metall. Trans. A., 12A, 1081 (1981).

12. Handbook of Auger Electron Spectroscopy, Second Edition (Physical Electronics Division, Perkin-Elmer Corporation (Eden Prairie, Minnesota, 1978).

13. C.M. Preece and A.R.C. Westwood, "Temperature-sensitive embrittlement of FCC metals by liquid metal solutions," Trans. ASM, 62, 418 (1962).

14. C.F. Old and P. Trevena, "Liquid metal embrittlement of aluminum single crystals by gallium," Met. Sci.J., 13 (1979).

15. W. Rostoker, J.M. McCaughey and J. Markus, Embrittlement by Liquid Metals (Reinhold, New York, 1960), pp. 28, 34, 36.

16. C. Roques-Carmes, M. Aucouturier and P. Lacombe, "The influence of testing temperature and thermal history on the intergranular embrittlement and penetration of aluminum by liquid gallium," Met. Sci. J., 7, 128 (1973).

17. J.R. Pickens, W. Precht, and A.R.C. Westwood, "Embrittlement of P/M X7091 and I/M 7175 aluminum alloys by mercury solutions," J. Mater. Sci., 18, 1872 (1983).

18. G.M. Scamans, "Intergranular stress corrosion cracking of aluminum alloys by hydrogen or by liquid metal embrittlement," Environmental Degradation of Engineering Materials Conference, eds., M.R. Louthan, Jr., R.P. McNitt, and R.D. Sissons Jr., (Blacksburg, VA, 1981), pp. 153-162.

19. N.J.H. Holroyd and D. Hardie, "Environmental-sensitive embrittlement of high strength aluminum alloys," in Hydrogen Effects in Metals, Proc. 3rd Int. Conf. on the Effect of Hydrogen on the Behavior of Materials (Jackson Lake, WY, 1980), pp. 449-457.

20. G.M. Scamans, R. Alani, and P.R. Swann, "Pre-exposure embrittlement and stress-corrosion failure in Al-Zn-Mg Alloys," Corr. Sci., 16, 443 (1976).

21. L. Montgrain and P.R. Swann, "Electron microscopy of hydrogen embrittlement in high purity Al-Zn-Mg alloy," in Hydrogen in Metals (Proc. Int. Conf. on the Effects of Hydrogen on Materials Properties and Selection and Structural Design, ASM (Champion, PA, 1973), pp. 575-584.

22. L. Christodoulou, "The role of hydrogen in environmental failure of high strength aluminum alloys," Ph.D. Thesis, Imperial College, London, Jan. 1980.

23. J.R. Pickens and T.J. Langan, "The effect of solution heat treatment temperature on grain boundary segregation and stress-corrosion cracking in Al-Zn-Mg alloys," to be submitted for publication in Metall. Trans. A.

24. L. Christodoulou and H.M. Flower, "In-situ H.V.E.M. observations of hydrogen embrittlement in Al-Zn-Mg alloys," in Hydrogen Effects in Metals, Proc. 3rd Int. Conf. on the Effect of Hydrogen on the Behavior of Materials (Jackson Lake, WY, 1980), pp. 493-501.

25. G.M. Scamans, "Hydrogen bubbles in embrittled Al-Zn-Mg alloys," J. Mater. Sci., 13, 27 (1978).

26. A.W. Thompson, "Ductile fracture topography: Geometrical contribution and effects of hydrogen," Metall. Trans. A., 10, 727 (1979).

27. J.L. Christian and J.F. Watson, "Properties of 7000 series aluminum alloys at cryogenic temperatures," Adv. Cryog. Eng., 6, 604 (1961).

28. J.G. Kaufman and E.T. Wanderer, "Tensile properties and notch toughness of some 7xxx alloys at -452°F," Adv. Cryog. Eng., 16, 27 (1970).

29. J.G. Kaufman, K.O. Bogardus, and E.T. Wanderer, "Tensile properties and notch toughness of aluminum alloys at -452°F in liquid helium," Adv. Cryog. Eng., 13, 294 (1967).

30. J. Hunter and G.M. Scamans, Alcan International Ltd., Banbury Research Laboratory, England, Unpublished results, October 1984.

31. W.G. Moffatt, The Handbook of Binary Phase Diagrams, vol. 3, General Electric Co., Corporate Research and Development (Schenectady, NY, 1984).

32. J.R. Pickens, J.R. Gordon, and L. Christodoulou, "Stress-corrosion cracking and hydrogen embrittlement in P/M x7091 and I/M 7095," in High Performance Aluminum Powder Metallurgy (Dallas, TX, 1982), pp. 177-192.

THE EFFECT OF SOLUTION HEAT TREATMENT ON GRAIN BOUNDARY SEGREGATION AND STRESS-CORROSION CRACKING OF Al-Zn-Mg ALLOYS

by:

J.R. Pickens and T.J. Langan
MARTIN MARIETTA CORPORATION
Martin Marietta Laboratories
1450 South Rolling Road
Baltimore, Maryland 21227

I. INTRODUCTION

The Al-Zn-Mg alloys (i.e., 7xxx series) are generally the strongest of the aluminum-base alloys. Unfortunately, their usefulness is often limited by susceptibility to stress-corrosion cracking (SCC). In fact, numerous SCC service failures of alloys in the series have been reported in peak-aged (i.e., T6-type tempers) thick sections, where short transverse stresses exist.[1] This susceptibility to SCC can be eliminated by overaging -- i.e., T7-type tempers -- but at a loss of about 15% in strength.

The mechanisms of SCC in Al-Zn-Mg alloys have been extensively studied to obtain insights into ways of decreasing SCC susceptibility of engineering 7xxx alloys. Furthermore, more ambitious studies have sought to eliminate susceptibility without paying the significant strength penalty that accompanies overaging. In addition, SCC of aluminum-base alloys is an intriguing phenomenon, and its mechanisms have been investigated for the insights they might provide into understanding environmentally assisted cracking in general.

According to the early view of the SCC mechanism in Al-Zn-Mg alloys, cracking occurs by anodic dissolution of the grain boundary (GB) region in aqueous environments.[2-4] However, reversible pre-exposure embrittlement,[5-10] observations of cracking in humid air containing too little moisture to effect dissolution,[11,12] greater susceptibility in Mode I than in Mode III[13-16], results of cathodic charging experiments,[17] and observations of cracking with no discernable GB precipitate dissolution on the SCC fracture surface[18,19] have collectively shown that hydrogen embrittlement (HE) is clearly involved in the SCC mechanism. In fact, recent work showing far greater crack velocity in Mode I than in Mode III for both Al-Mg[20] and Al-Zn-Mg[14,15,21,22] alloys led investigators to conclude that most of the crack advance during SCC is by HE, not dissolution.

SCC of Al-Zn-Mg alloys is most often intergranular, so numerous studies have focused on GB segregation in these alloys. For example, Doig and Edington[23,24] used electron energy loss measurements (EELS) and X-ray microanalysis in a transmission electron microscope (TEM) to show that Mg and Zn concentration profiles across the precipitate-free zone (PFZ) and the GB vary greatly depending on heat treatment and quench rate. However, this technique provides limited spatial resolution and only limited information on the composition of the actual GB surface. Green et al.,[25] Chen et al.,[26] Viswanadham et al.,[27] and Sun et al.[28,29] endeavored to use the extreme surface sensitivity of Auger electron spectroscopy (AES) to obtain segregation information on the actual grain boundary. Specimens of various Al-Zn-Mg and Al-Zn-Mg-Cu alloys were fractured under ultra-high vacuum (UHV) at approximately -194°C, and GB segregation was measured from the resultant intergranular fractures. They obtained information from about 6-8 grains under the electron beam and concluded that both Mg and Zn segregate to the boundaries, with the Zn largely bound in $MgZn_2$ precipitates, but with a significant portion of the Mg atoms existing "freely" on the boundaries. The presence of this "free Mg" in the region where cracking occurs and the great affinity of Mg for hydrogen led Viswanadham et al.[27] and Scamans[18] to independently propose, in general terms, a Mg-H interaction mechanism of SCC. Recently, Langan and Pickens[30] have observed fine dimples on the intergranular fracture surface of Al-Zn-Mg alloys fractured at -194°C, showing that the fracture is not entirely on the actual GB surface, but likely in the PFZ. Thus, in the studies where free Mg was claimed to have been observed, much of the segregation data likely were not obtained from the boundaries. Consequently, there is some uncertainty as to whether free Mg does indeed exist on grain boundaries.

The various theories of how Mg or Zn atoms segregate to the boundaries have recently been reviewed.[31] One school of thought suggests that the solute atoms experience "equilibrium segregation" at the boundaries during solution heat-treatment. This theory predicts that segregation decreases with

increasing solution heat-treatment temperature (SHT). Alternatively, one "non-equilibrium segregation" school of thought suggests that solute atoms interact with vacancies and migrate to the boundaries during high-temperature heat treatment or quenching and subsequent aging. This theory predicts that segregation increases with increasing SHT. Consequently, the role of SHT in GB segregation and SCC susceptibility has been studied by several investigators, but unfortunately changes in alloy compositions from one study to another make direct comparisons difficult.

Taylor and Edgar[32] qualitatively assessed GB segregation in solutionized and quenched Al-Zn-Mg alloys on which anodic films were grown. Localized reduction in thickness at the intersection of the film and the boundaries would be taken as evidence of elemental GB segregation. Such attack was observed and increased in severity with increasing bulk Mg content, but was largely insensitive to change in bulk Zn content. This was considered as indirect evidence of Mg segregation during solutionizing. Furthermore, they observed that the amount of segregation decreased with increasing SHT as would be expected from equilibrium segregation models. Taylor and Edgar also assessed the SCC resistance of Al-4.4Zn-1.8Mg* alloy specimens that were solutionized, water-quenched (WQ), naturally aged for 35 days, and then cold rolled 50%, by measuring time-to-failure (ttf) as a function of SHT. They found that ttf increased in the SHT range from 425 to 525°C, where it reached a maximum, and then decreased at the highest SHT studied -- 575°C.

Vlasova et al.[33] studied the effect of SHT on the SCC behavior of an Al-5.5Zn-1.8Mg alloy. They found that in the solutionized, water-quenched, and artificially aged condition, ttf decreased monotonically with SHT in the range of 360-600°C. For specimens that were air-cooled and either naturally or artificially aged, ttf was constant for $360 < SHT < 460$°C, and then decreased with SHT up to 600°C.

*Unless otherwise noted, all compositional values are in wt%.

Scamans[34] measured GB segregation on Al-Zn-Mg-Cu commercial alloy 7079 using X-ray photospectroscopy (XPS). Specimens were pre-exposed to liquid gallium and then fractured in air before examination under UHV. The specimens were solution heat treated at either 400 or 510°C, and water-quenched prior to measuring segregation to avoid including contributions from the Mg and Zn atoms in the GB precipitates. Scamans found Mg segregation on the boundaries in the as-quenched condition. Furthermore, more Mg was found at the lower SHT, which is consistent with the equilibrium theory of segregation. Scamans also noted that this difference in segregation is consistent with the reduced reactivity of GB-surface intersections of Al-Zn-Mg alloys in water vapor when solutionized at a higher temperature. However, a subsequent observation by Langan and Pickens[30] suggests that inducing intergranular fracture by pre-exposure to liquid gallium makes accurate measurement of Mg concentration difficult. They observed Ga-Mg interactions on Ga-embrittled Al-Zn-Mg fracture surfaces that led to an increase in the measured Mg with increasing time after fracture.

Joshi et al.[35] and Shastry, Joshi, and Levy[36] assessed the SCC susceptibility of Al-Zn-Mg-Cu alloy 7075 using bolt-loaded double cantilever beam (DCB) specimens. Plateau crack velocity was taken as a measure of SCC propagation susceptibility, which is particularly relevant for studies relating GB segregation to SCC. They measured plateau velocity for specimens in the T6 condition (solutionized, water-quenched, artificially aged to peak strength) and found that plateau velocity decreased with SHT from 393 to 438°C, where it passed through a minimum, and then increased with SHT up to 527°C. In addition, segregation of Zn, Mg, and Cu was measured using AES on specimens fractured in liquid nitrogen environments (i.e., the previously described method[25-29]) and they found that all three elements were present on the boundaries. Segregation of Mg, Zn, and Cu each passed through a minimum at a SHT of 438°C, the SHT where plateau velocity was minimum.

Thus, there is no general agreement on the effect of SHT on the SCC susceptibility of Al-Zn-Mg alloys. In fact, the results of Taylor and

Edgar[32] and Scamans[34] are largely opposite to those obtained by Vlasova et al.,[33] and both sets of SCC data[32,33] used smooth, non-precracked specimens, in which crack growth is both propagation and initiation dependent. Accordingly, the objectives of the present work are to:

- Measure SCC susceptibility as a function of SHT using both a propagation-dependent test and one having both initiation and propagation dependence.

- Measure GB segregation in an Al-Zn-Mg alloy by AES from in-situ fractures on the actual GB surfaces.

- Elucidate the mechanism of SCC by determining if grain boundary segregation is a necessary precursor to stress corrosion susceptibility.

II. MATERIALS AND EXPERIMENTAL PROCEDURES

A. ALLOY L

A high-purity alloy was designed to be extremely SCC susceptible so data could be acquired in a relatively short period of time. The alloy is a nominal Al-6.9Zn-2.9Mg-0.1Zr (Al-3.0at%Zn-3.3at%Mg-0.03at%Zr) alloy (composition in Table I), which has approximately the same Zn and Mg contents as 7178, a commercial alloy known to exhibit severe SCC susceptibility in the peak-aged condition. The Zr was added for grain refinement instead of Cr, which is often used in 7xxx aluminum alloys, because Cr-containing dispersoids reportedly reduce SCC susceptibility by interacting with hydrogen during SCC.[37] Our hope is to avoid this potential complication and concentrate on the segregation of Mg and Zn. The alloy was chill-cast in a 13.3 x 13.3 x 25.4 cm (5.25 x 5.25 x 10 in.) mold using 99.994% pure aluminum. An aging curve was developed at 121°C after an SHT of 475°C (Fig. 1). The following thermo-mechanical processing scheme was carefully designed to isolate SHT and its effect on GB segregation as a variable.

1. Homogenize ingot: 19.5 h at 427°C (800°F)
   7.5 h at 465°C (870°F)
   slow furnace cool.

2. Roll ingot to produce susceptible, pancake-grain morphology. Roll at 380°C (720°F) from 13.2 cm to 3.2 cm in 12 passes [final pass 320°C (608°F)]. WQ* to minimize static recrystallization.

---

* All water quenching was performed in ice water at 0°C.

TABLE I

Alloy Compositions

Alloy		Zn	Mg	Zr	Impurities	Al
L	wt%	6.92	2.85	0.125	<0.01	Balance
	at%	3.00	3.30	0.03	---	Balance
G	wt%	4.40	3.70	0.00	<0.01	Balance
	at%	1.80	4.20	0.00	---	Balance

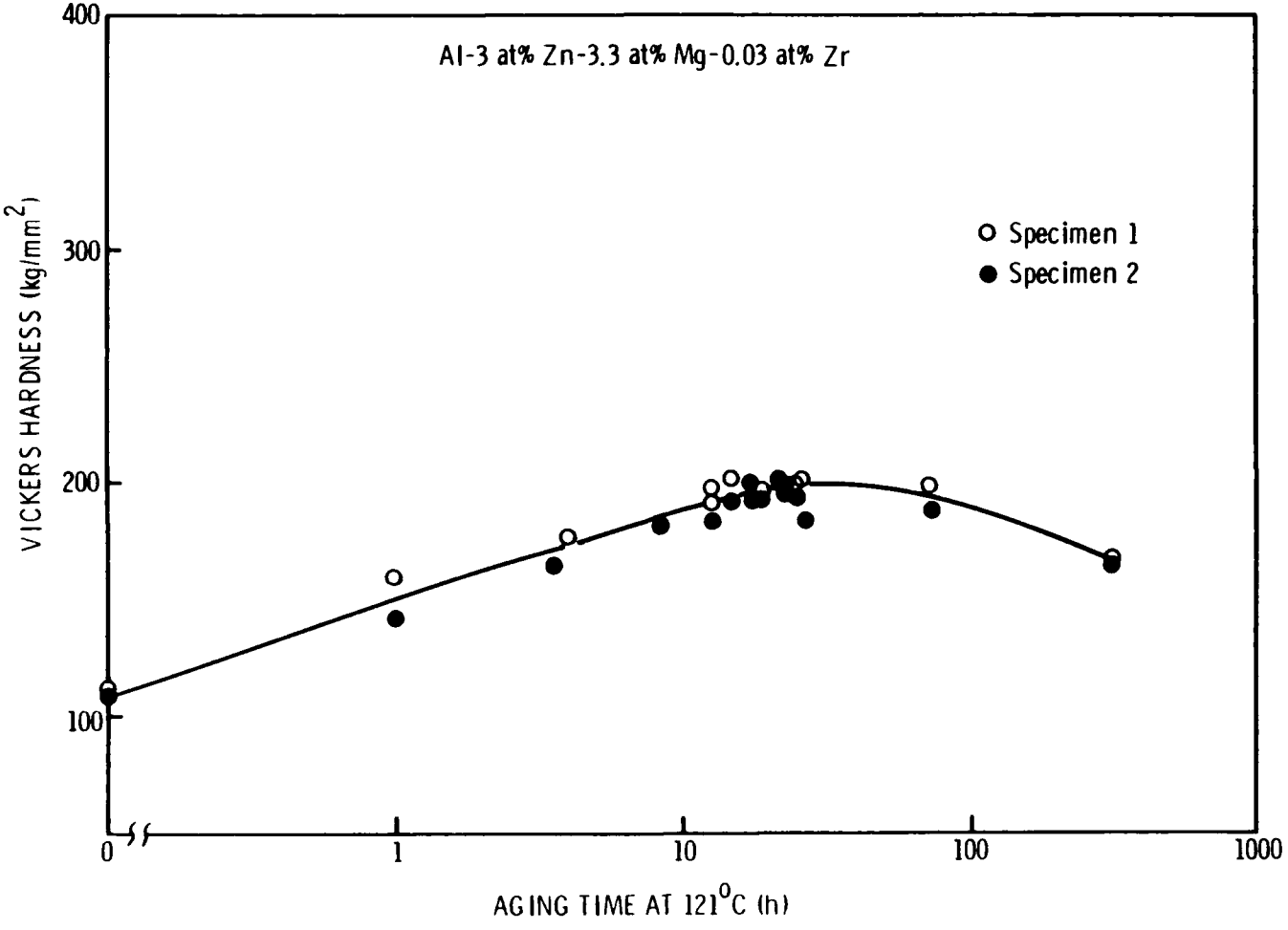

Figure 1. Aging curve for Al-6.9Zn-2.9Mg-0.12Zr (wt%) alloy L at 121°C after solutionizing at 475°C and ice water quenching.

3. Heat to 515°C, hold for 2 h, to uniformly induce any recrystallization that is going to occur. WQ. Machine 18 x 3 x 1.5 cm blanks in the S-L orientation[38] from the center of the plate where the grains are most uniform.

4. Age at 170°C for 8 h to remove by precipitation any equilibrium segregation that may have occurred during solutionizing at 515°C.

5. Solution heat treat at 475°C. WQ and perform aging study at 121°C to determine time to achieve peak-age strength. Based on these results (Fig. 1) peak strength was obtained by aging at 121°C for 20h.

6. Solution heat treat for 2 h at selected temperatures, WQ, age at 121°C for 20 h to peak strength. (Measure hardness for each SHT specimen to ensure that the aging condition used produces the same strength in each specimen.)

7. Machine DCB specimens (12.7 x 2.54 x 1.27 cm) from the oversized blanks to remove sufficient material to eliminate residual stresses introduced by quenching.

8. Machine Auger fracture specimens from each blank so that segregation measurements are performed on the same heat-treated specimens as are used for the SCC data.

B. ALLOY G

A high-purity Al-4.4Zn-3.7Mg (Al-1.8at%Zn-4.2at%Mg) alloy (composition in Table I) was also used for assessing SCC susceptibility as a function of SHT. This alloy was available in 1.5-mm (0.060 in.) thick sheet and was

machined into smooth 7.62-cm (3.00-in.) dogbone specimens having a 5.12 x 0.64 x 0.15 cm (2.0 x 0.25 x 0.060 in.) test section. This alloy has a 170-μm, equiaxed, mean grain diameter. The specimens were solutionized at various temperatures, water-quenched, and aged for 24 h at 121°C, which produced peak hardness.[39]

C. BOLT-LOADED DCB TEST FOR SCC

The bolt-loaded DCB test was performed according to techniques developed by Speidel[11] and Speidel and Hyatt.[40] The DCB specimens were precracked at 30% of K_{IC} and a compliance calibration was performed on this alloy. This calibration provides K_I as a function of crack length, which was measured using a travelling microscope.

The DCB specimens were subjected to alternate immersion in the following environment: 0.6M (3.5 wt%) NaCl + 0.02M $Na_2Cr_2O_7$ + 0.07M $NaC_2H_3O_2$ and sufficient $HC_2H_3O_2$ to obtain pH = 4. This solution (chromate-inhibited brine, hereafter) was developed by Sprowls et al.[41] to simulate seawater SCC and inhibit general corrosion, thereby preserving fracture surfaces for examination.

D. STRESS-TTF SCC TESTS USING UNNOTCHED SPECIMENS

The alloy G specimens were loaded to 240 MPa (35 ksi), which is 80% of the yield strength, under constant immersion in the chromate-inhibited brine solution. Time-to-failure was measured from 5 specimens at each of four SHTs.

E. SEGREGATION MEASUREMENTS

Auger fracture specimens from peak-aged alloy L that were solutionized at 440, 460, 475, 490, and 515°C, and those solutionized at 475°C but aged for various times at 121°C, were subjected to pre-exposure embrittlement to induce

intergranular fracture. The fracture pins were charged with hydrogen by exposure to water vapor-saturated air (WVSA) at 100°C for 8 h at 1 atmosphere gauge pressure (15 psig) and then fractured under UHV in the chamber of a Physical Electronics model 595 scanning Auger microprobe (SAM). The specimens were fractured by impact and the 1000-2000Å diameter probe placed as soon as possible on a featureless, intergranular facet.

Survey scans were performed, and the peak-to-peak heights were measured for Mg, Al, and Zn from the differentiated spectra. These heights were corrected using published sensitivity factors[42] and the following ratios were computed: Mg/(Mg+Zn+Al), Al/(Mg+Zn+Al), and Zn/(Mg+Zn+Al). In these ratios, each elemental symbol signifies the corrected peak-to-peak height for the element. These ratios are taken as a semiquantitative estimate of the atomic fraction on the fracture surface.

Scanning electron microscopy (SEM) was used to assess the intergranular nature of fractures from both the pre-exposure embrittled Auger specimens, and the SCC surfaces of the DCBs. In addition, transmission electron microscopy was used to characterize the grain boundary precipitates.

III. RESULTS

The hardness of the alloy L specimens aged for 20 h at 121°C, but solutionized at different temperatures, was essentially constant (see Table II). Thus, differences in SHT did not have a significant effect on aging behavior. The SCC plateau velocity of alloy L decreased with increasing SHT (Fig. 2). Reliable K_{ISCC} values could not be measured because of the severe SCC susceptibility of alloy L. Crack arrest was often equivocal. For the smooth, sheet tensile specimens of alloy G, ttf increased with increasing SHT (Fig. 3). Each of these trends indicates decreasing SCC susceptibility with increasing SHT.

Segregation measurements were made from over 130 regions of peak-aged alloy L specimens that were solutionized at the five temperatures. Magnesium segregation was observed on the GBs as evidenced by the significantly greater value of Mg/(Mg+Zn+Al) there than in the grain interior (Fig. 4). The grain interior value was obtained from a survey scan performed after sputtering a polished cross section of alloy L. Although the data for individual GBs are scattered, it is clear that the value of Mg/(Mg+Zn+Al) on the boundary is several times greater than that in the bulk. Although significant variation in Mg/(Mg+Zn+Al) occurred on the various GBs, the mean value of this parameter was approximately equal for all SHTs (Fig. 4).

Zinc was present on the boundaries (Fig. 5) in amounts somewhat higher than that in the grain interiors. The mean value of Zn/(Mg+Zn+Al) was approximately the same for all SHTs.

If one assumes that all the Zn atoms on the boundaries are bound in the $MgZn_2$ precipitates, then the parameter (Mg - 1/2 Zn)/(Mg+Zn+Al) would be a measure of free Mg on the boundaries. Auger survey scans were performed on a stoichiometric $MgZn_2$ crystal and verified that the Zn:Mg peak-to-peak ratio, corrected using published sensitivity factors, is 2:1. From the plot of this free Mg parameter vs SHT (Fig. 6), it is clear that there is "free-Mg" on the

TABLE II

Hardness Values for Alloy L DCB Specimens[a]

SHT (°C)	Rockwell B	Vickers (kg/mm^2)
440	85.5	197
460	86.0	196
475	87.2	190
490	87.0	192
515	85.8	193

---

[a] Each specimen was solutionized for 2 h at the temperature noted, ice water-quenched, and aged for 20 h at 121°C.

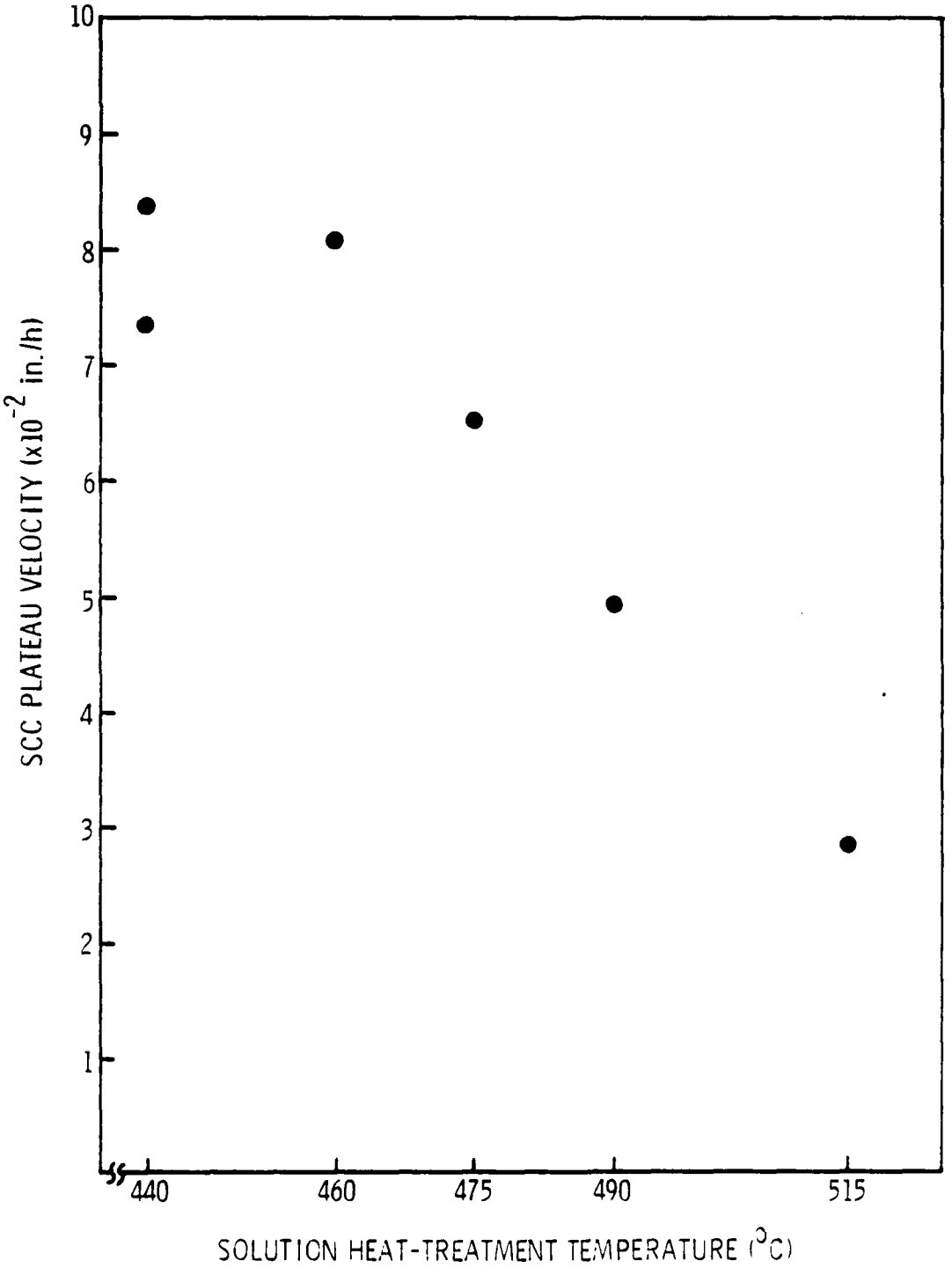

Figure 2. Stress-corrosion plateau velocity vs solution heat-treatment temperature for peak-aged Al-6.9Zn-2.9Mg-0.1Zr (wt%) alloy L.

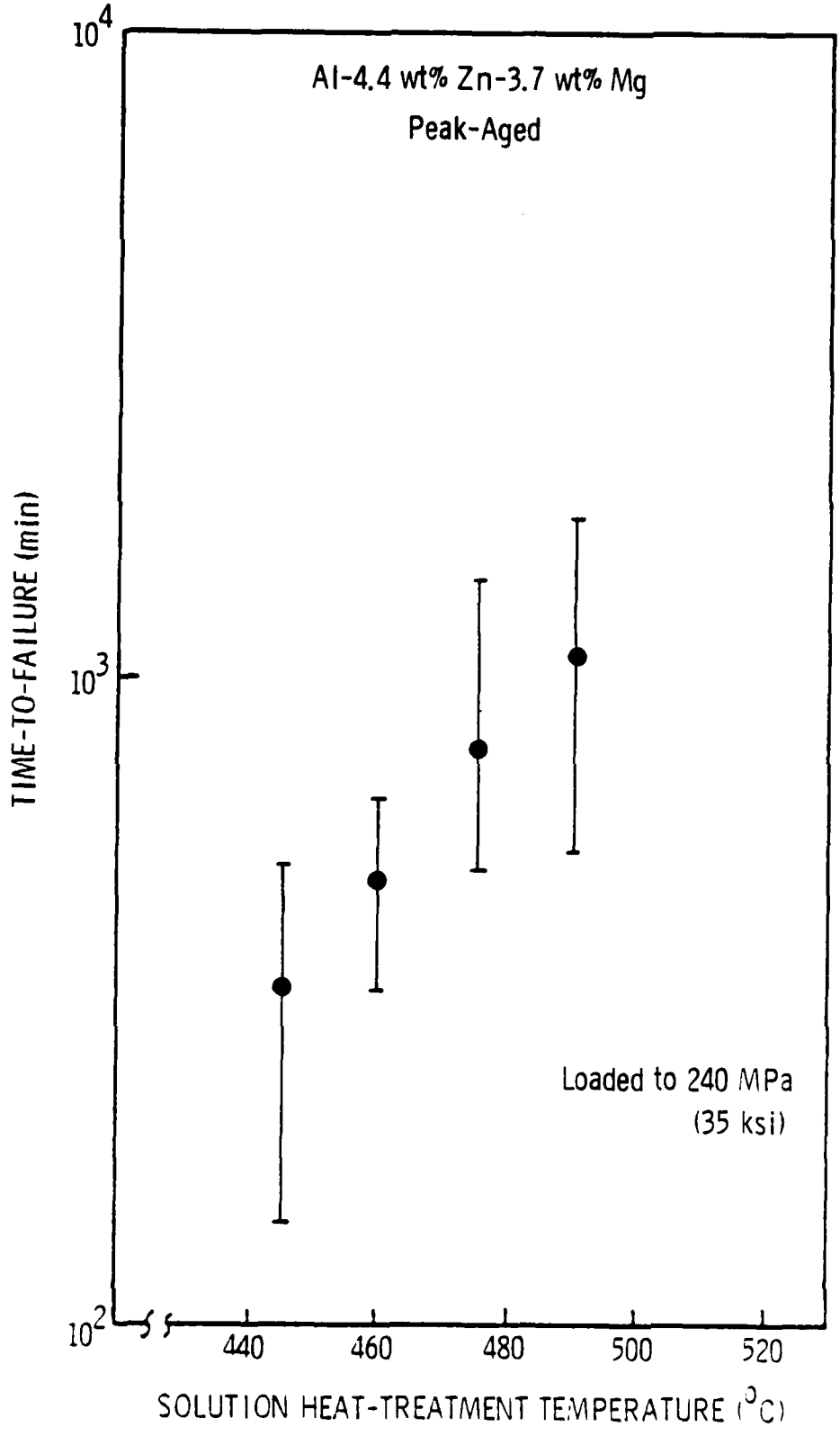

Figure 3. Time-to-failure vs solution heat-treatment temperature for peak-aged Al-4.4Zn-3.7Mg (wt%) alloy G.

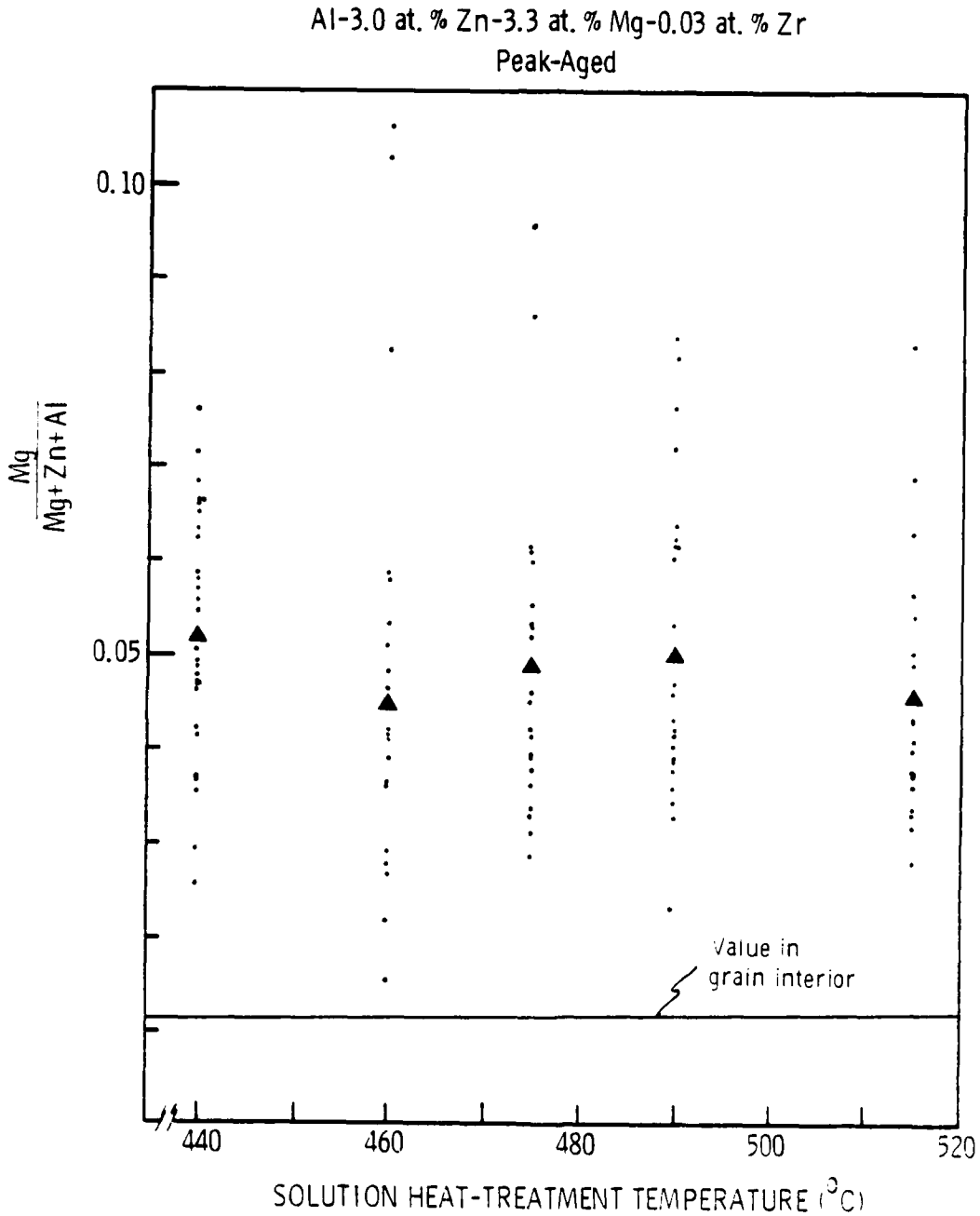

Figure 4. Magnesium segregation vs solution heat-treatment temperature for Al-6.9Zn-2.9Mg-0.1Zr (wt%) alloy L.

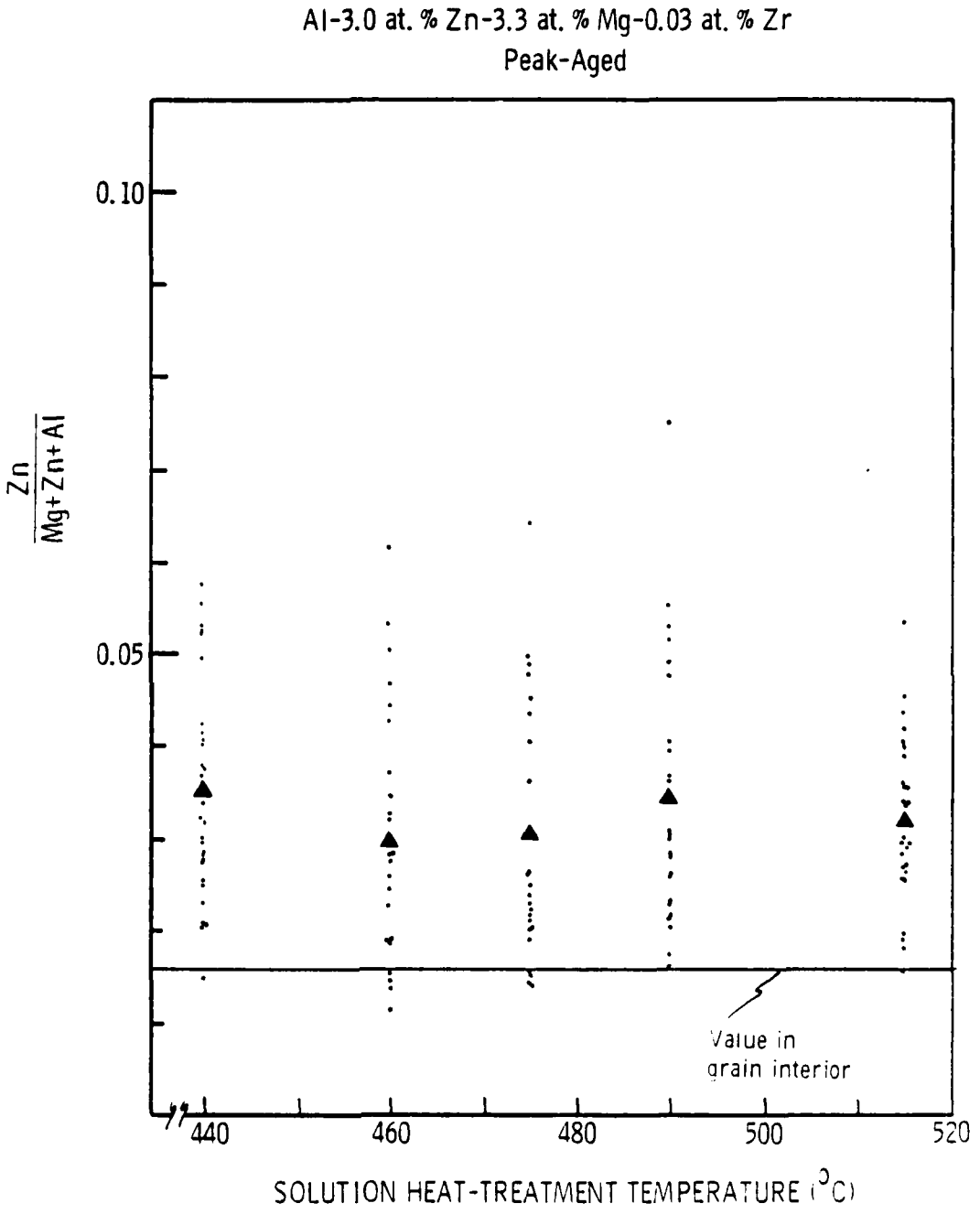

Figure 5. Zinc segregation vs. solution heat-treatment temperature for peak-aged Al-6.9Zn-2.9Mg-0.1Zr (wt%) alloy L.

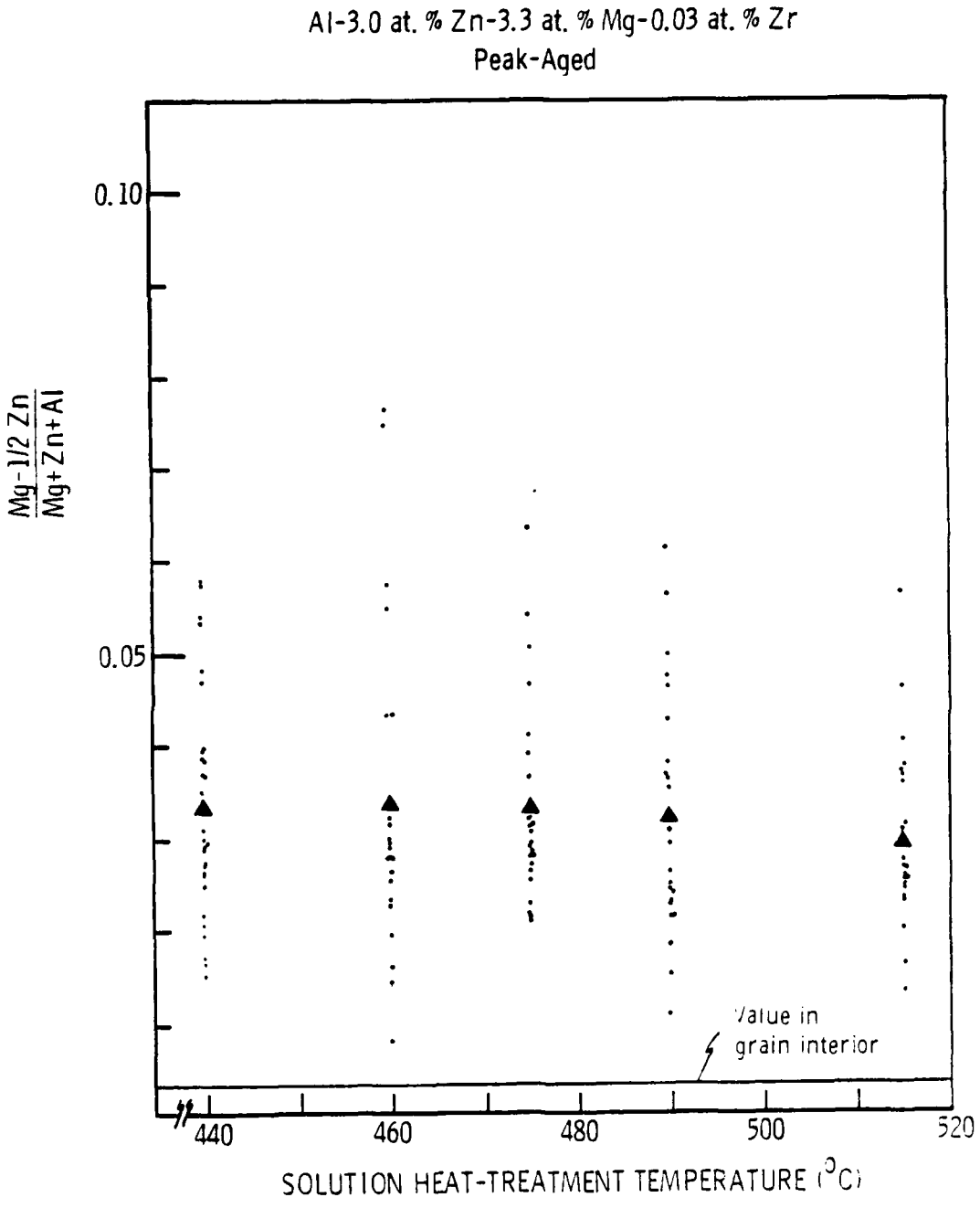

Figure 6. Free magnesium parameter vs solution heat-treatment temperature for peak-aged Al-6.9Zn-2.9Mg-0.1Zr (wt%) alloy L.

boundaries, and that its concentration is essentially independent of SHT. We emphasize that this assumes that "free Zn" does not exist, as claimed by Sun et al.,[28] Chen et al.,[26] and Viswanadham et al.[27] Nevertheless, if some Zn atoms were not bound in the $MgZn_2$ precipitates, then there would be even more "free Mg" than is shown in Fig. 6.

The fracture surfaces of the pre-exposure-embrittled Auger fracture pins were mostly intergranular (Fig. 7a) and contained mostly featureless regions, as can be seen at high magnification (Fig. 7b). A cross section of a typical fractured pin reveals secondary intergranular cracking just below the main fracture surface (Fig. 8a). At high magnifications, the crack can be seen to propagate along the actual boundary (Fig. 8b). To the 30Å resolution limit of our scanning electron microscope, we conclude that large regions of the fracture path on pre-exposed specimens are on the actual GB.

The SCC fracture path also is largely intergranular and greatly resembles that of the pre-exposure embrittled Auger fracture specimens (compare Figs. 7a and 9).

The GBs of alloy L at any given SHT were extremely varied in appearance, ranging from high-angle GBs with extensive precipitation (Fig. 10) to low-angle boundaries with some precipitation (Fig. 11). No differences in GB precipitation between the various SHT specimens were apparent, although statistical stereological analysis was not performed.

The SCC susceptibilities of alloy L specimens that were solutionized to 475°C and aged for 20 or 100 h at 121°C were similar, and no susceptibility was observed for specimens aged 300 h (Fig. 12).

Segregation measurements from in situ fractures revealed no clear trend in Mg/(Mg+Al+Zn) as a function of aging time at 121°C for material solutionized at 475°C (Fig. 13). However, Zn/(Mg+Al+Zn) decreased monotonically from the as-quenched condition to the overaged condition (300 h at 121°C) (Fig. 14), and (Mg - 1/2 Zn)/(Mg+Al+Zn) was largely independent of aging (Fig. 15).

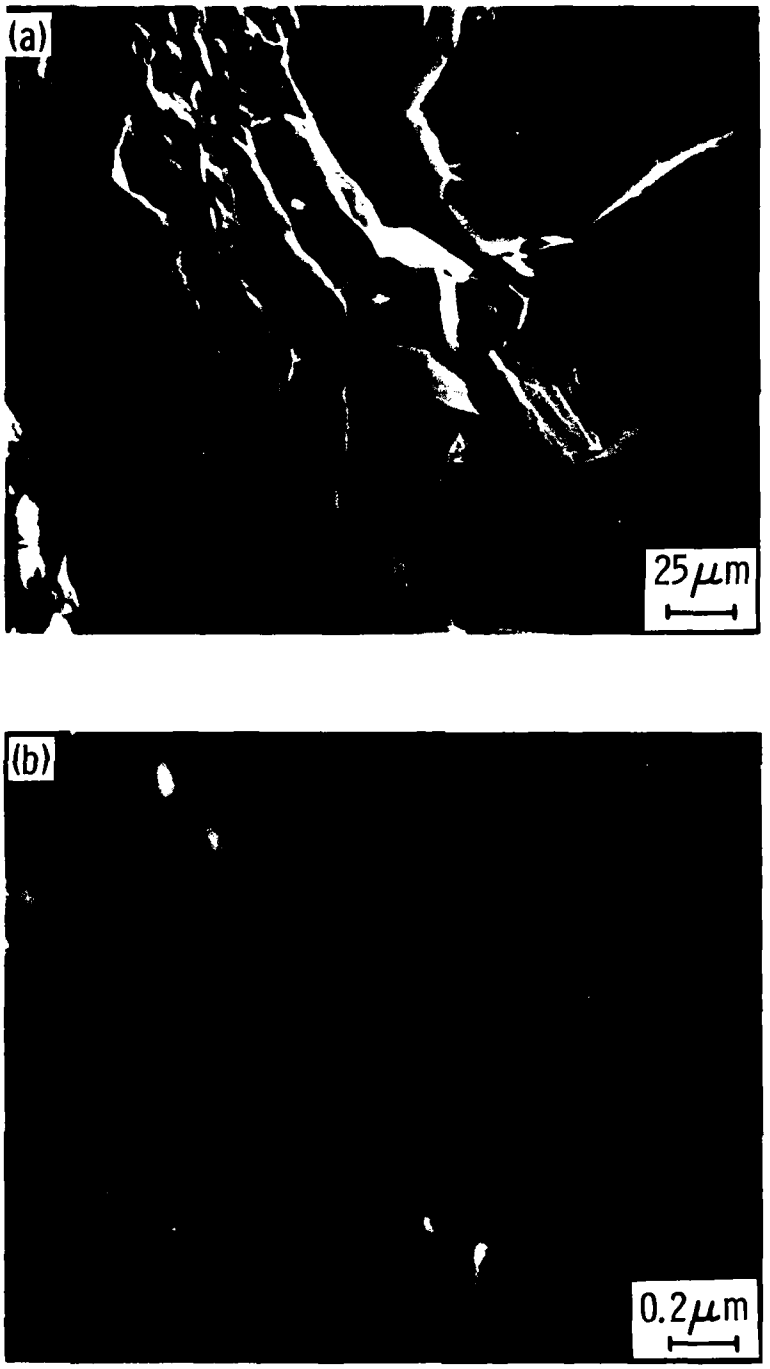

Figure 7. Intergranular pre-exposure-embrittled Auger fracture specimen a) has regions that are completely featureless at high magnification b).

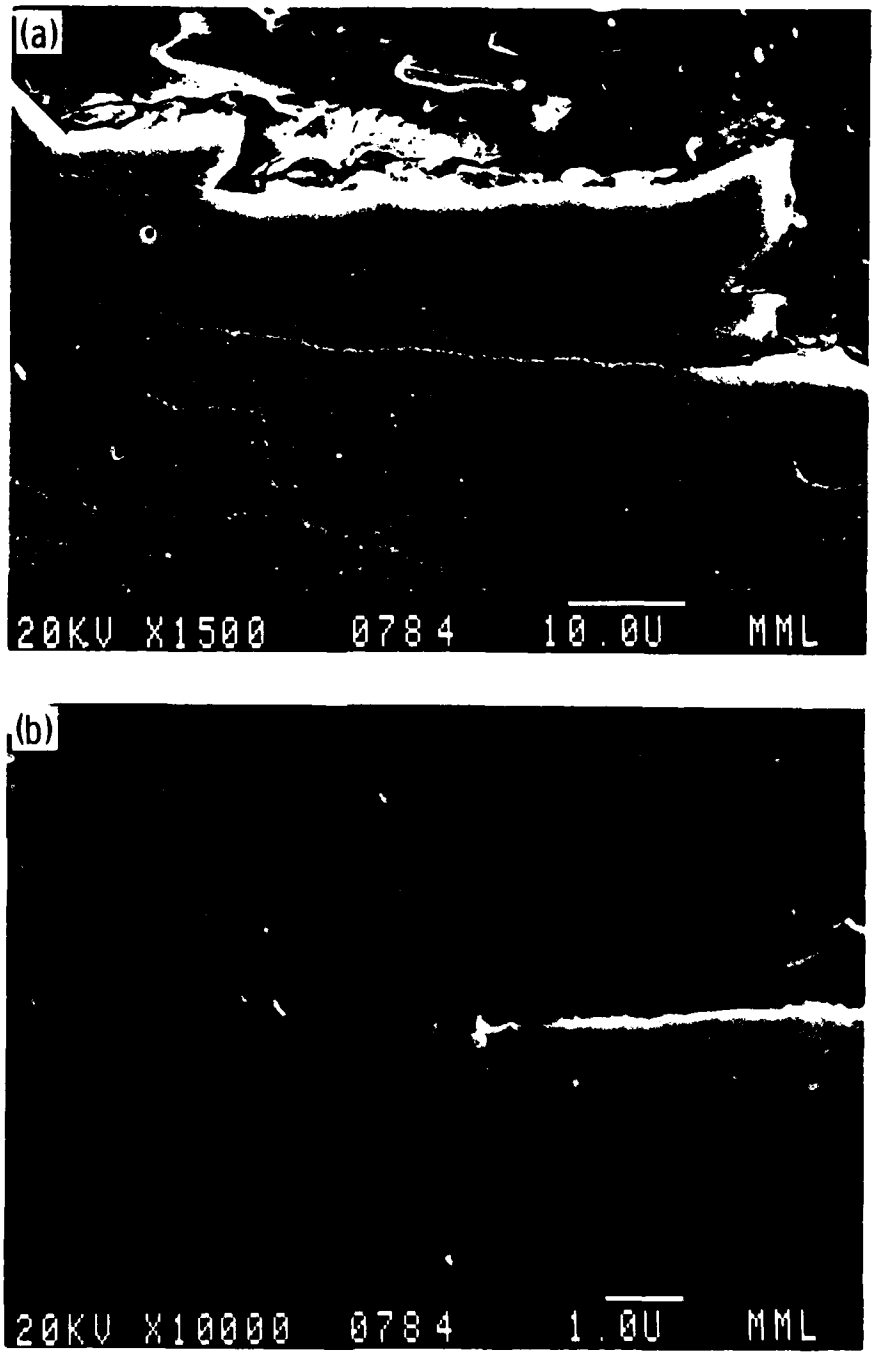

Figure 8. Cross section of Auger specimen fractured after pre-exposure embrittlement showing intergranular fracture at a) intermediate and b) high magnification.

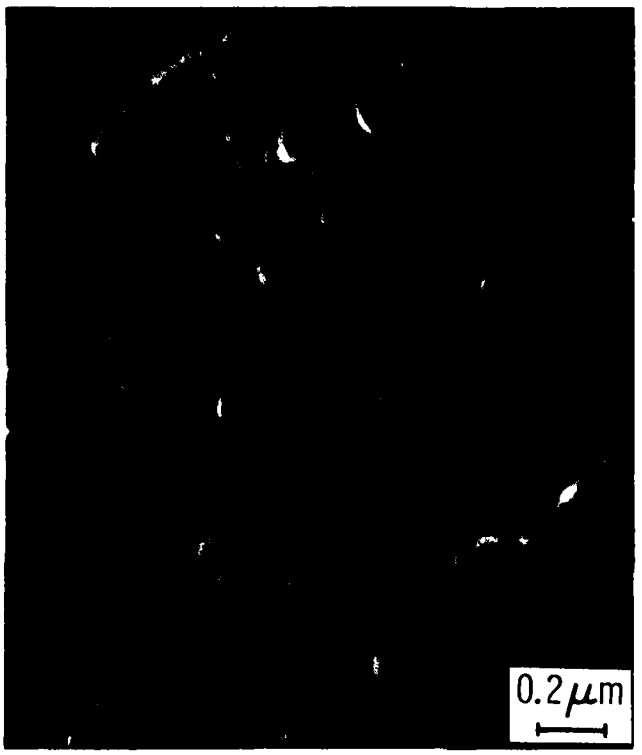

Figure 9. The SCC fracture path on Al-6.9Zn-2.9Mg-0.12Zr (wt%) alloy L is largely intergranular, and is very similar to the pre-exposure embrittlement fracture surface (see Fig. 7a).

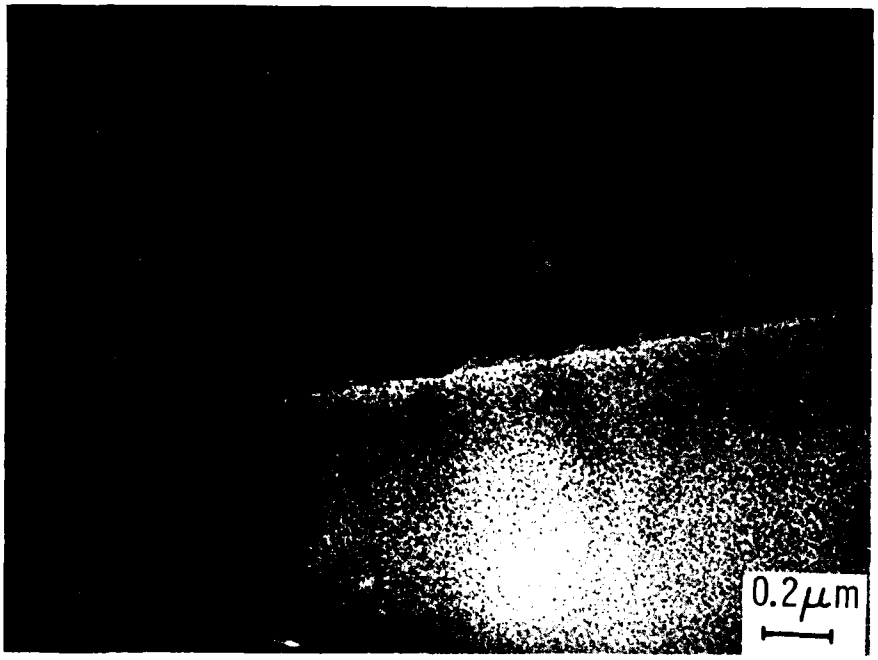

Figure 10. Transmission electron micrograph of high-angle grain boundary of Al-6.9Zn-2.9Mg-0.12Zr (wt%) alloy L.

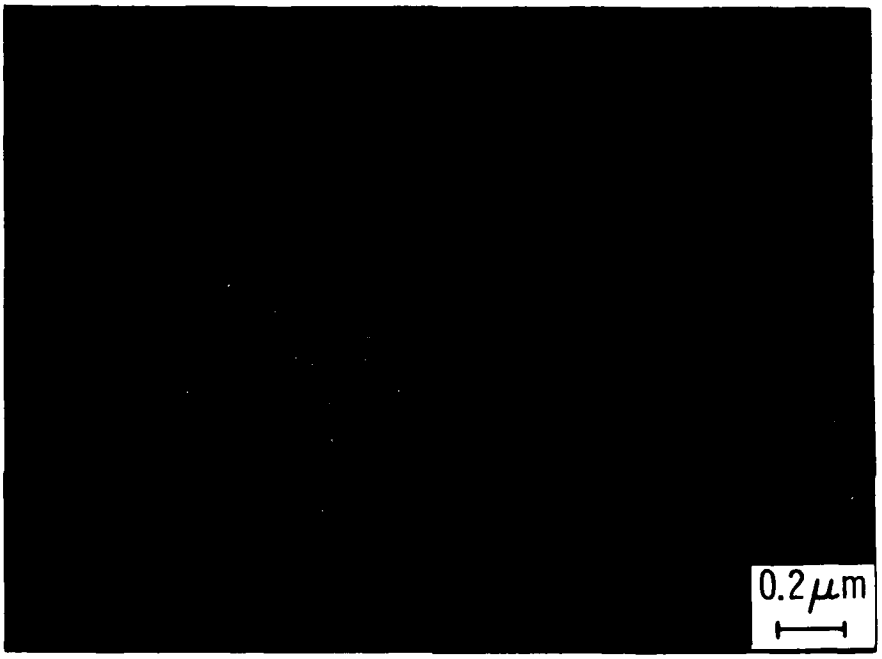

Figure 11. Transmission electron micrograph of low-angle grain boundary of Al-6.9Zn-2.9Mg-0.12Zr (wt%) alloy L showing precipitation.

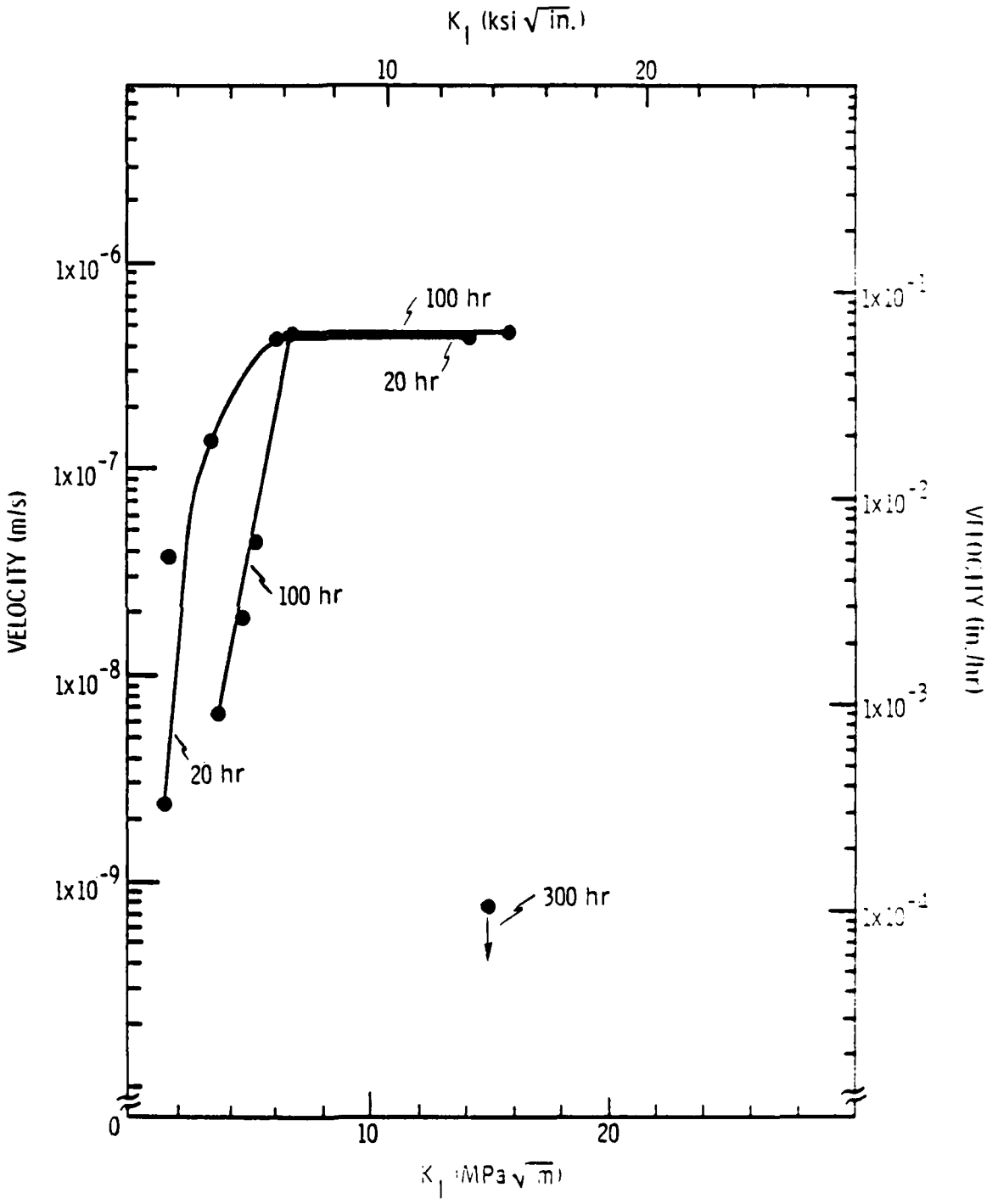

Figure 12. Stress-corrosion velocity vs Mode I stress intensity for specimens solutionized at 475°C, water-quenched, and aged for various times at 121°C.

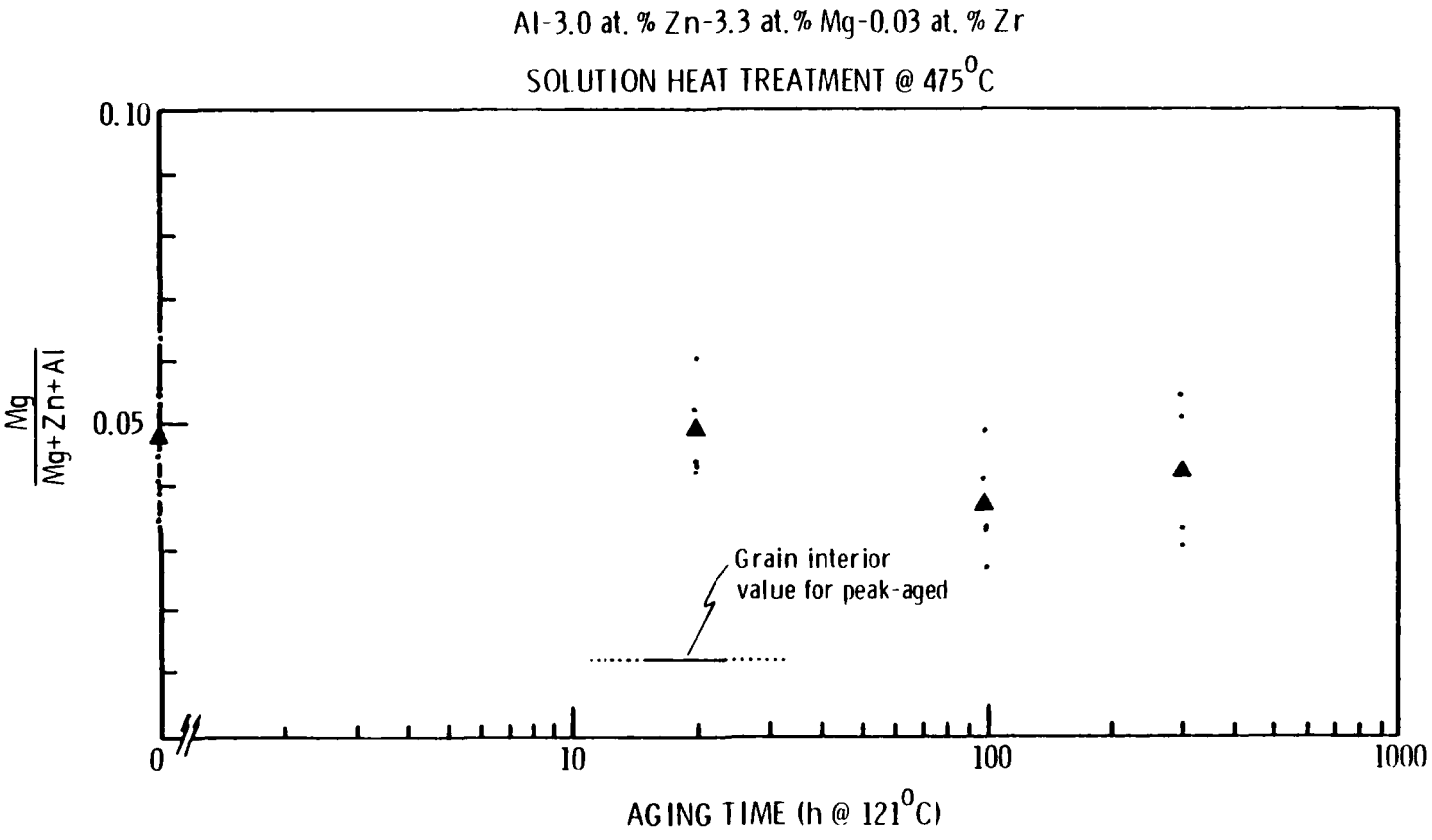

Figure 13. Magnesium segregation vs aging time at 120°C for alloy L specimens solutionized at 475°C and water-quenched prior to aging.

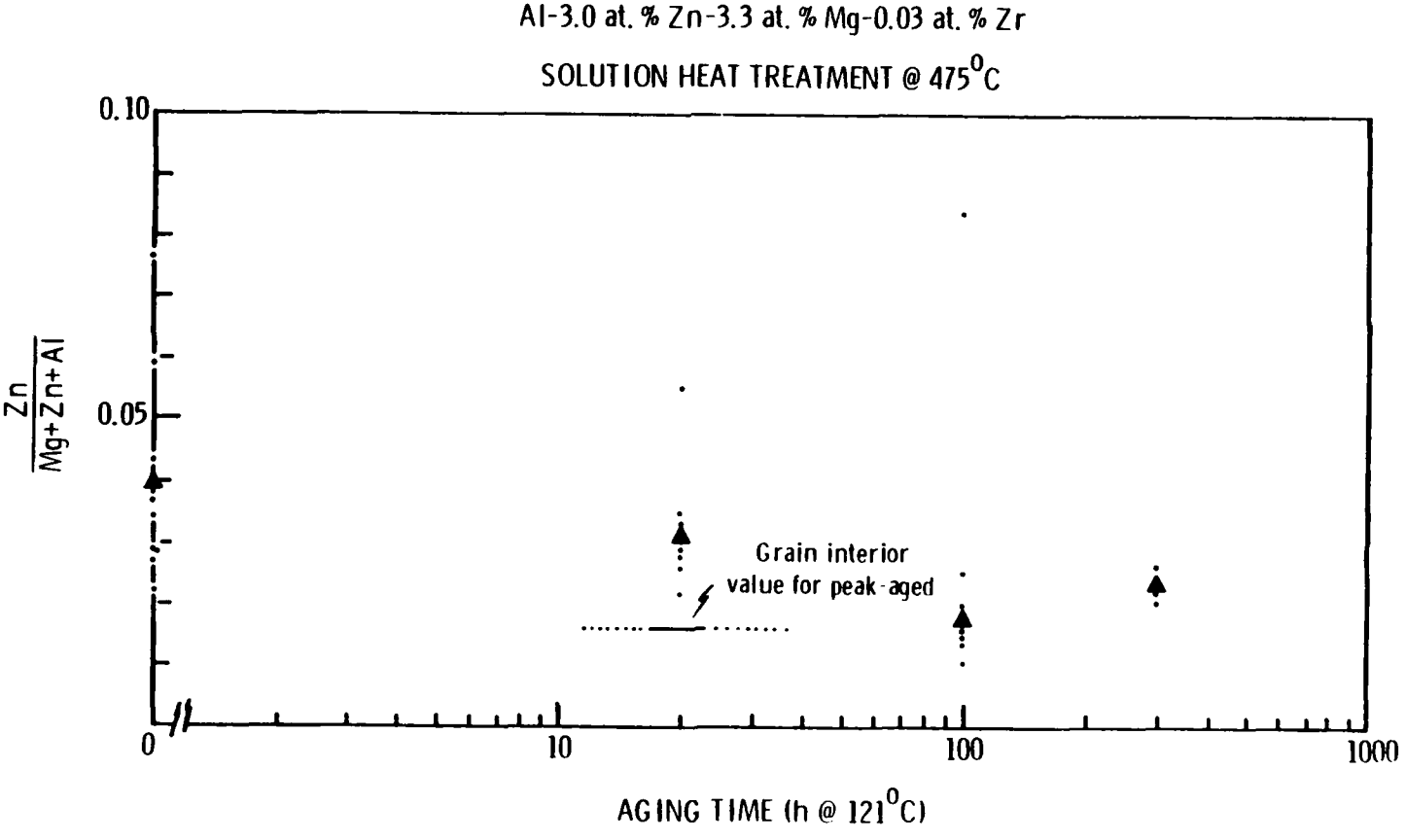

Figure 14. Zinc segregation vs aging time at 121°C for alloy L specimens solutionized at 475°C, and water-quenched prior to aging.

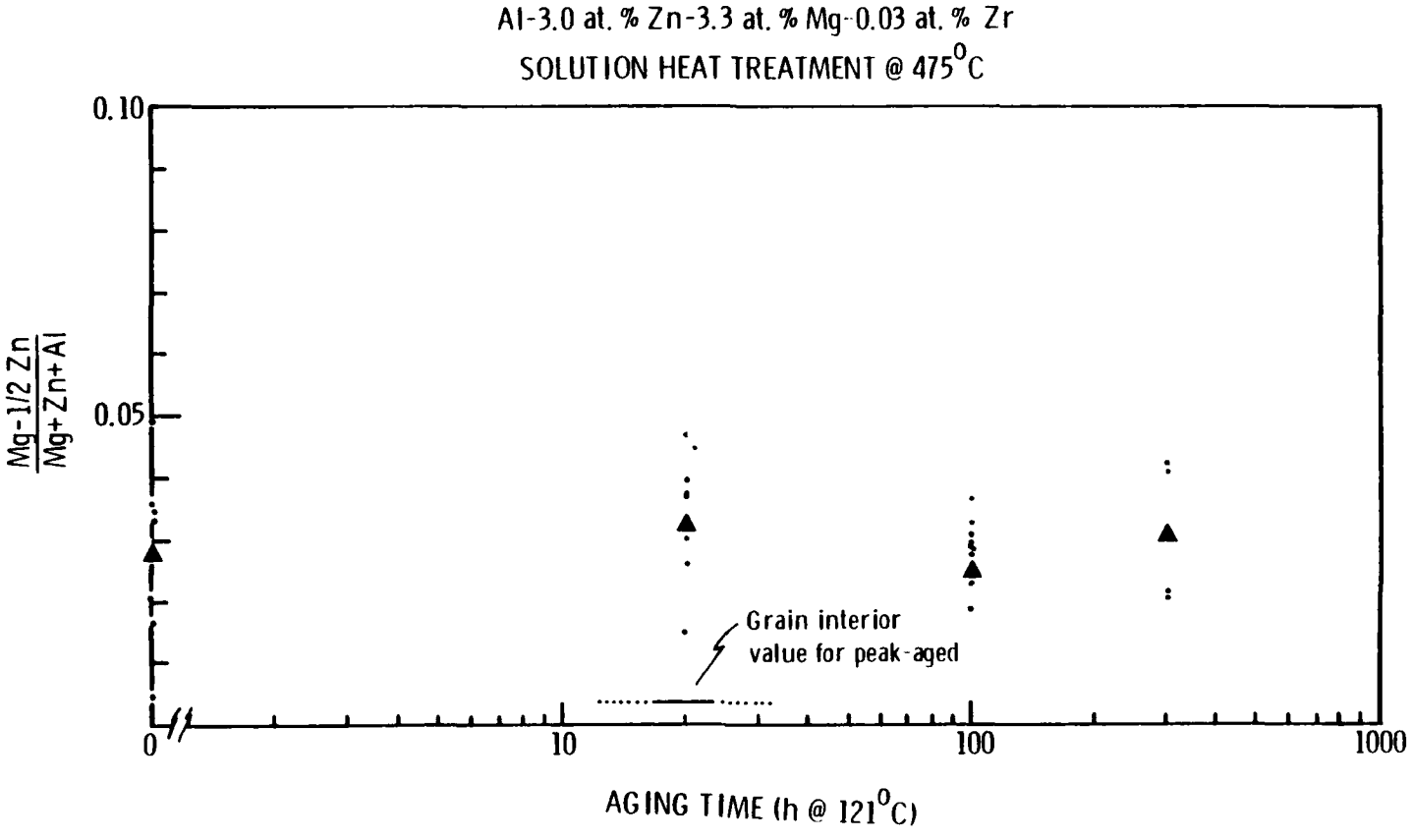

Figure 15. Free-magnesium parameter vs aging time at 121°C for alloy L specimens solutionized at 475°C, and water-quenched prior to aging.

IV. DISCUSSION

The decrease in SCC susceptibility with increasing SHT obtained for both alloy L precracked DCB specimens and for smooth alloy G specimens is consistent with the work of Taylor and Edgar[32] and Scamans,[34] but opposite that of Vlasova et al.[33] In addition to changes in segregation, many factors that affect SCC susceptibility can be altered by variations in SHT. For example, grain size can change by grain growth or static recrystallization. Furthermore, the substructure of the alloy can change by static recovery. Along with these subtle changes, it must also be noted that none of these SHT studies were carried out on alloys with exactly the same composition [e.g., various Zn/Mg ratios, different total solute contents (wt%Zn+wt%Mg), and some contained copper]. Consequently, it would be easy to speculate on why different investigators have observed different trends in susceptibility with SHT. We can only emphasize that in the present work, we were as careful as possible in isolating SHT and its effect on segregation as an independent variable.

The work that is perhaps most comparable to ours is that done by Joshi et al.[35] and Shastry, Joshi, and Levy[36] on commercial Al-Zn-Mg-Cu alloy, 7075. They found that GB segregation of Mg, Zn, and Cu all pass through a minimum at a SHT of 438°C and, furthermore, that plateau velocity is also minimum at this SHT. Joshi et al. attribute their segregation results to the competition between equilibrium and non-equilibrium segregation. Equilibrium segregation models predict that solute atoms segregate to the boundaries during solutionizing, and that this segregation decreases with increasing SHT. The non-equilibrium segregation model predicts that segregation occurs during quenching and aging; the quenched-in vacancies interact with solute atoms and drag them to the boundaries where the vacancies are annihilated. Because the equilibrium vacancy concentration increases with increasing

temperature, non-equilibrium segregation is predicted to increase with increasing SHT. Thus, the competition between these two segregation mechanisms was used by Joshi et al. to explain the segregation minimum observed.

The specimens Joshi et al.[35] used for Auger analysis were fractured at cryogenic temperatures, and in our earlier work we showed that the resulting fracture path is largely dimpled, and not completely on the actual grain boundary surface. In fact, Joshi et al. recognized this fact and evidence of plasticity can be seen on the intergranular facets shown in their publication. Consequently, we suspect that their segregation data contain information from the PFZ as well as from the actual boundary. Also, Joshi et al.[35] used a 5-μm probe which provides information averaged over a larger area than the 1000-2000 Å probe used in the present work. Perhaps the variation in segregation on individual boundaries led to sufficient scatter in the present results to mask trends in segregation. In fact, Malis and Chaturverdi[43] used microanalysis to measure Mg segregation in an Al-8Mg alloy and found great variation in Mg content as they moved along a given boundary. Nevertheless, the differences in plateau velocity and segregation vs SHT between the work of Joshi et al. and the present work are significant.

In the present work, free Mg has been unequivocally shown to exist on the boundaries of an Al-Zn-Mg alloy. That is, fracture was on the boundary surface and measurements were taken from dimple-free regions. This is in contrast to the dimpled intergranular surfaces that are characteristic of fracture at cryogenic temperatures. We did not, however, find a correlation between free Mg segregation, (Mg - 1/2 Zn)/(Mg+Al+Zn), and SCC susceptibility as would be expected from the Mg-H mechanism proposed by Viswanadham et al.[27] and Scamans.[34] Perhaps the boundaries of this alloy are so saturated with "free Mg" that enough is present to contribute to the cracking mechanism, and any excess has no effect.

There is no apparent explanation for the decrease in SCC susceptibility with increasing SHT. Examination by transmission electron microscopy of the

grain boundary precipitate size and spacing for the various SHTs revealed no apparent differences. We can only speculate on reasons for the variation in susceptibility as follows:

1. A subtle decrease in free Mg does exist with increasing SHT that was not discerned because of scatter.

2. The mean GB precipitate size is coarser or the mean free path between the precipitates increases with increasing SHT, but to an extent that could only be discerned by performing extensive quantitative microscopy of many grain boundaries.

3. Although the free Mg concentration on the boundaries is essentially independent of SHT, high localized segregation may be more prevalent on the GBs of specimens subjected to lower SHTs, thus increasing their SCC susceptibility. These localized regions would probably be to narrow to be detected by SAM.

Schmiedel and Gruhl[44,45] have recently claimed that the amount of Zn segregation on the GBs correlates more closely with SCC susceptibility than does the Mg segregation. They base this claim on plots showing a good correlation between ttf and segregation, as measured by X-ray microanalysis, for both Mg and Zn in alloys with bulk Zn/Mg weight percent ratios less than 2.9, but for alloys with bulk compositions larger than 3, only the Zn segregation shows good correlation with ttf. Our observation of decreasing Zn/(Mg+Al+Zn) with increased aging time (Fig. 15) is consistent with their second conclusion. However, in light of our finding of approximately twice as much Mg as Zn on the boundary, both Mg and Zn atoms would have to be "free" for there to be a Zn-H interaction analogous to the proposed Mg-H interaction.[27,34] In view of previous work, we are surprised that measured Mg segregation did not vary with SHT or aging time. It is possible that the

515°C SHT -- the temperature to which all specimens were exposed to uniformly induce any static recrystallization that was going to occur -- saturated the boundaries with Mg atoms which were not removed by subsequent lower temperature SHT. This effect could mask any trends in Mg segregation with SHT.

It is also possible that the effects of equilibrium and non-equilibrium segregation are balanced, so that segregation does not vary with SHT as proposed by Joshi et al.[35] In other words, perhaps equilibrium segregation occurring during solutionizing results in decreasing Mg and Zn segregation with increasing SHT. However, at high SHTs, the concentration of quenched-in vacancies is greater, so non-equilibrium segregation occurring by vacancy drag increases with increasing SHT. The segregation measurements on the specimens solutionized at various temperatures were performed in the peak-aged temper, so it is possible that the two types of segregation, having opposite temperature dependencies, actually resulted in similar segregation as a function of SHT.

V. CONCLUSIONS

1. Susceptibility to SCC decreases with increasing solution heat-treatment temperature for both an Al-6.8Zn-3.0Mg-0.1Zr and an Al-4.4Zn-3.7Mg alloy (wt%). For the former alloy, solution heat-treatment temperature and its effect on segregation were carefully controlled.

2. Mg and Zn segregation occur on the grain boundaries of Al-Zn-Mg alloys. There are about 50% more Mg than Zn atoms on the boundaries, even though the equilibrium $MgZn_2$ precipitates have 2 Zn atoms for each Mg atom. Consequently, free Mg atoms exist on the boundaries.

3. No correlation between Mg segregation and SCC susceptibility could be found. Consequently, the previously proposed magnesium-hydrogen interaction mechanism of SCC remains unproven.

VI. ACKNOWLEDGEMENTS

The authors appreciate the technical assistance in obtaining Auger data of Drs. A. Taylor, and G.T.K. Swami, and Mr. H. Erskine at the National Science Foundation-sponsored facility at the University of Minnesota. We also appreciate the helpful scientific discussions with Drs. G.M. Scamans, N.J.H. Holroyd, A. Joshi, T.S. Sun, and J.A.S. Green, and Mr. J. Goss. Finally, we are grateful to the Office of Naval Research for sponsoring research under contract N00014-83-C-0380 and to Dr. P. Clarkin for his long-standing support.

VII. REFERENCES

1. M.O. Speidel: Metall. Trans. A, 1975, vol. 6A, p. 631.

2. D.O. Sprowls and R.H. Brown: Fundamental Aspects of Stress-Corrosion Cracking, p. 466f, Conf. Proc., Ohio State Univ., Natl. Asso. Corros. Eng., Houston, TX, 1969.

3. A.J. Sedriks, J.A.S. Green, and D.L. Novak: Metall. Trans., 1970, vol. 1, p. 1815.

4. R.B. Mears, R.H. Brown, and E.H. Dix, Jr.: Symposium on Stress-Corrosion of Metals, p. 329ff, ASTM/AIME, 1944.

5. W. Gruhl: Z. Metallkd., 1963, vol. 54, p. 86.

6. W. Gruhl and H. Cordier: Z. Metallkd, 1964, vol. 55, p. 577.

7. L. Montgrain and P.R. Swann: in Hydrogen in Metals, p. 575, Proc. Int. Conf. Effects of Hydrogen on Materials Properties and Selection and Structural Design, ASM, Champion, PA, 1973.

8. R. Alani and P.R. Swann: B. Corros. J., 1977, vol. 12, no. 2 p. 80.

9. G.M. Scamans, R. Alani, and P.R. Swann: Corros. Sci., 1976, vol. 16, no. 7, p. 443.

10. G.M. Scamans and C.D.S. Tuck: Environment-Sensitive Fracture of Eng. Materials, TMS/AIME, NY, 1979.

11. M.O. Speidel: The Theory of Stress Corrosion Cracking in Alloys, p. 289, Nato Science Committee, 1971.

12. M.O. Speidel: Hydrogen in Metals, p. 23, ASM, Proc. Int. Conf. Effects of Hydrogen on Materials Properties and Selection and Structural Design, Champion, PA, 1973.

13. J.A.S. Green, H.W. Hayden, and W.G. Montague: Effect of Hydrogen on Behavior of Materials, p. 200, AIME, Philadelphia, PA, 1976.

14. J.R. Pickens, J.R. Gordon, and L. Christodoulou: High Performance Aluminum Powder Metallurgy, p. 177, TMS-AIME, 1983.

15. J.R. Pickens: Rapidly Solidified Powder Aluminum Alloys, ASTM Committee B-9, Philadelphia Centre Hotel, PA, 1984.

16. R.E. Swanson, I.M. Bernstein, and A.W. Thompson: Scr. Metall., 1982, vol. 16, p. 321.

17. R.J. Gest and A.R. Troiano: Corrosion-NACE, 1974, vol. 30, no. 2, p. 274.

18. G.M. Scamans: Scr. Metall., 1979, vol. 13, p. 245.

19. G.M. Scamans: Metall. Trans. A, 1980, vol. 11A, p. 846.

20. J.R. Pickens, J.R. Gordon, and L. Christodoulou: High Performance Aluminum Powder Metallurgy, p. 177, TMS-AIME, 1982.

21. J.R. Pickens and L. Christodoulou: Metall. Trans. A (in publication).

22. J.R. Pickens, L. Christodoulou, and T.J. Langan: Final Report on Army Research Office Contract No. DAAG-29-81-C-0031, November 1983.

23. P. Doig and J.W. Edington: Corrosion NACE, 1975, vol. 31, no. 10, p. 347.

24. P. Doig and J.W. Edington: Br. Corros. J. (Quarterly), 1974, vol. 9, no. 4, p. 220.

25. J.A.S. Green, R.K. Viswanadham, T.S. Sun, and W.G. Montague: Corrosion/77, Proc. Int. Corrosion Forum, paper 17, p. 17/1, Natl. Assoc. Corros. Eng., San Francisco, CA, 1977.

26. J.M. Chen, T.S. Sun, R.K. Viswanadham, and J.A.S. Green: Metall. Trans. A, 1977, vol. 8A, p. 1935.

27. R.K. Viswanadham, T.S. Sun, and J.A.S. Green: Metall. Trans. A, 1980, vol. 11a, p. 85.

28. T.S. Sun, J.M. Chen, R.K. Viswanadham, and J.A.S. Green: Appl. Phys. Lett., 1977, vol. 31, no. 9, p. 580.

29. T.S. Sun, J.M. Chen, R.K. Viswanadham, and J.A.S. Green: J. Vac. Sci. Technol., vol. 16, no. 2, p. 668.

30. T.J. Langan and J.R. Pickens: to be submitted for publication, Mater. Sci. Eng.

31. G.M. Scamans, N.J.H. Holroyd, and C.D.S. Tuck: Preprint received in private communication with G.M. Scamans, Alcan Banbury Research Lab, Banbury, UK.

32. I.T. Taylor and R.L. Edgar: Metall. Trans., 1971, vol. 2, p. 833.

33. T.A. Vlasova, E.K. Zenkova, L.N. Polyakova and V.E. Silis: Fiz. Met. Metalloved., 1967, vol. 23, no. 2, p. 357.

34. G.M. Scamans: Environmental Degradation of Engineering Materials in Aggressive Environments, p. 153, Virginia Polytechnic Institute Press, Blacksburg, VA, 1981.

35. A. Joshi, C.R. Shastry, and M. Levy: Metall. Trans. A, 1981, vol. 12A, p. 1081.

36. C.R. Shastry, M. Levy, and A. Joshi: Corro. Sci., 1981, vol. 21, no. 9, p. 673.

37. L. Christodoulou: Ph.D. Thesis, 1980, Imperial College, London,

38. American Society for Testing and Materials, 1980 Annual Book of ASTM Standards, ASTM E399-789, Part 10, p. 580, 1980.

39. J.R. Pickens, D. Venables, and J.A.S. Green: End of Year Report on Office of Naval Research Contract No. N00014-74-C-0277, P00007, January 1981.

40. M.O. Speidel and M.V. Hyatt: Advances in Corrosion Science and Technology, vol. 2, p. 115, Plenum Press, NY, 1972.

41. D.O. Sprowls, M.B. Shumaker, J.W. Coursen, and J.D. Walsh: Final Report, Part I (1968-1972), Contract No. NAS 8-21487, for George C. Marshall Space Flight Center, May 31, 1973.

42. Handbook of Auger Electron Spectroscopy (2nd ed.), Physical Electronics Division, Perkin-Elmer Corp., Eden Prairie, MN, 1978.

43. T. Malis and M.C. Chaturverdi: J. Mater. Sci., 1982, vol. 17, p. 1479.

44. H. Schmeidel and W. Gruhl: Metall. Jahrgang, 1984, vol. 38, no. 1, p. 32.

45. H. Schmiedel and W. Gruhl: Z. Metallkd., 1983, vol. 74, No. 12, p. 777.

END

DTIC

4-86